

2D MoS₂: structure, mechanisms, and photocatalytic applications

N. Thomas ^{a, b, d}, S. Mathew ^{a, b, d}, K.M. Nair ^{a, b}, K. O'Dowd ^{a, b}, P. Forouzandeh ^{a, b}, A. Goswami ^{b, c}, G. McGranaghan ^{b, c}, S.C. Pillai ^{a, b, *}

^a Nanotechnology and Bio-engineering Research Group, Department of Environmental Science, Institute of Technology Sligo, Sligo, Ireland

^b Centre for Precision Engineering, Materials and Manufacturing Research (PEM), Institute of Technology Sligo, Sligo, Ireland

^c Department of Mechanical and Manufacturing Engineering, Institute of Technology, Sligo, Ireland



ARTICLE INFO

Article history:

Received 4 February 2021
Received in revised form
29 March 2021
Accepted 31 May 2021
Available online 7 June 2021

Keywords:

2D MoS₂ composites
Morphology
Photo-electrochemistry
Contaminant degradation
Disinfection
Antibiotic-resistant organisms

ABSTRACT

Two-dimensional (2D) molybdenum disulfide (MoS₂)–based materials are of great interest because of their capacity to efficiently absorb electromagnetic spectrum in the visible region. Starting from the structural and electronic properties, this review discusses the synthesis strategies of 2D MoS₂. The major photocatalytic applications of 2D MoS₂ such as hydrogen evolution, pollutant degradation, self-cleaning, photoelectrochemical water splitting, and microbial disinfection are summarized. The mechanistic understanding of various photocatalytic applications of 2D MoS₂ is summarized through schematic diagrams. In addition, this review outlines the methodologies for improving the 2D MoS₂ photocatalysts and recapitulates the research directions in this area of semiconductor photocatalysis.

© 2021 The Authors. Published by Elsevier Ltd. This is an open access article under the CC BY license (<http://creativecommons.org/licenses/by/4.0/>).

1. Introduction

Semiconductor photocatalysis is widely applied for solving a number of environmental problems such as energy shortage and pollution [1]. TiO₂ is reported as the most explored material for photocatalytic applications. Because the pristine TiO₂ primarily absorbs the electromagnetic spectrum in the ultraviolet (UV) region, this hinders the broad applications of pristine TiO₂ materials [2]. Recent decades have witnessed a surge in the number of studies reported on photocatalytic applications of semiconductor materials such as g-C₃N₄, molybdenum disulfide (MoS₂), and ZnO [3,4]. Among them, MoS₂ semiconductor material is of significant interest because of its excellent optical absorption property and fast charge carrier dynamics [5].

The crystal structure of bulk MoS₂ consists of a vertical arrangement of MoS₂ layers connected by weak van der Waals interactions [6–8]. The bulk MoS₂ material is reported to have an indirect bandgap of 1.2 eV, whereas two-dimensional (2D) single-layer MoS₂ nanosheets have a direct bandgap of 1.8 eV [9,10]. The

absorption spectrum of 2D MoS₂ falls in the visible region of the electromagnetic spectrum, and this opens up an ocean of opportunities for widespread applications [10]. MoS₂-based materials are reported to have applications in the area such as energy storage [11], hydrogen production [12], degradation of contaminants [13], disinfection [14], etc. Recently, many researchers have summarized the photocatalytic characteristics of MoS₂ for various categories of applications [5,15–18]. Yet, there are no recent reviews available in the literature that briefly summarize the recent advances in the photocatalytic strategies and applications of 2D MoS₂-based materials. In this review, the authors outline the state-of-the-art research directions in 2D MoS₂ photocatalysis and the possible future trends that the researchers should adopt for the practical applications of MoS₂ photocatalysis.

2. Structural understanding: crystal structure, electronic and optical properties

MoS₂ is a class of layered 2D transition metal dichalcogenides (TMDCs), with the chemical formula of MX₂. M denotes the transition metal element, and X denotes S, Se, or Te [8,20]. The bulk TMDCs are formed by stacking of X-M-X layers and can exist in different structural phases depending on the transitional metal atoms [7]. In single-layered MoS₂ films, the Mo (+4) and S (-2) are

* Corresponding author.

E-mail address: pillai.suresh@itsligo.ie (S.C. Pillai).

^d Both authors contributed equally to this manuscript.

arranged in S–Mo–S orientation, and in each layer, 6 S atoms surround one Mo atom. MoS₂ generally exists in two structural phases: either trigonal prismatic (2H/3R) or octahedral (1T). Structural phases depend on the stacking arrangement of layers in MoS₂ with respect to Mo coordination (Fig. 1). The 2H structure is the dominant stable phase observed in nature with the ABA layer stacking and has two layers per unit cell oriented in hexagonal symmetry [21]. Here, the sulfur atoms from different atomic planes occupy the same positions perpendicular to each other. The Mo–S bond is predominantly covalent, whereas the S layers are coupled by van der Waals interactions and slide effortlessly against each layer [22]. This structural property helps to cleave crystals along with the surface layers (Z direction) by breaking weak van der Waals forces, and this property is exploited in the synthesis of single-layered MoS₂ [23,24].

Synthetically prepared MoS₂ commonly shows a 3R structure, where it has a rhombohedral symmetry with three layers per unit cell and is highly unstable. This structure can rearrange the orientation into 2H type under heating. In the 2H and 3R MoS₂ structures, Mo hexagonal arrays are sandwiched between the sulfur layers [25]. The 1T crystal structure has an ABC layering order and is formed by the disorientation of one of the sulfur layers in MoS₂ [26]. It has a symmetrical Mo–Mo bond and has a trigonal symmetry, also known as the metallic 1T phase (Fig. 1). The electrical conductivity of MoS₂ differs with respect to the phase and crystal structure. 1T phases have more exposed active sites; thus, the presence of 1T enhances the electrical conductivity of the MoS₂ [21].

The band structure of material changes, while varying from the three-dimensional (3D) bulk counterpart to 2D sheets of MoS₂. The number of layers in the MoS₂ determines the physical and chemical properties of the material. The bulk MoS₂ shows a direct bandgap of 1.3 eV [27], whereas the monolayer MoS₂ exhibits an indirect bandgap of 1.9 eV [8]. This phenomenon can depend on quantum confinement, interlayer interactions, and long-range Coulomb effects [28,29].

Several density functional theory (DFT) studies have been performed to understand the electronic characteristics in MoS₂ [30–33]. As shown in Fig. 2, for the bulk counterpart, an indirect bandgap is presented between the r, valence band (VB) maximum point, and the K (Brillouin zone point), which is the minimum point

in the conduction band (CB). In the figure, the CB and VB edges are denoted by red and blue lines, respectively. The molybdenum d-orbitals attribute to the K value, and no change will occur in this value as the size decreases because it is not affected by the number of layers. 2p orbitals of sulfur form the VB. Thus, the bandgap between K and r fluctuates, as it is formed by hybridized orbitals of p_z and d orbitals of S and Mo, respectively. As the number of layers decreases, the VB maximum (VBM) point r decreases below zero, to form a new VBM point. The lowest energy transition is vertical, i.e. direct for the monolayer, and the energy needed for the indirect transition in the monolayer is larger than the direct band edge transition. The newly formed bandgap between the steady K point and new r will have an increased gap of 1.9 eV.

Apart from the number of layers, the crystal structure also has a significant influence on the band structure of MoS₂. The 2H phase displays semiconductor properties because of the presence of filled d_{2g} and empty d_{xy} and d_{x²-y²} orbitals. In contrast, the 1T phase shows metallic behavior as its 4 d² orbitals split into e_g orbitals other than t_{2g} orbitals. The two electrons filled in t_{2g} states give rise to the metallic character of 1T. The charge mobility of the material is also drastically increased by the thinness of the material and a direct bandgap introduction, as bulk MoS₂ requires higher energy to move electrons from the VB to the CB. Because of the dependence of the number of layers on optical properties, MoS₂ can be engineered for different applications by intercalation, reducing dimensions, or forming various heterostructures [15].

The changes in the structural parameters while progressing from 3D to 2D structure can be analyzed by Raman spectroscopy. Under infrared scattering, MoS₂ has four Raman active modes, E_{1g}, E_{2g}¹, A_{1g}, and E_{2g}², where the prominent peaks are E_{2g}¹ and A_{1g} (Fig. 3a). From the characteristic wavelength of the Raman spectra, the structure of the MoS₂ can be analyzed. For the bulk MoS₂ (3D), the E_{2g}¹ has a value of 383 cm⁻¹ and A_{1g} has a value of 408 cm⁻¹. The 2D monolayer MoS₂ shows the E_{2g}¹ and A_{1g} peaks at the value of 385 cm⁻¹ and 404 cm⁻¹, respectively. E_{2g}¹ denotes the in-plane opposite vibration of S atoms, and the out-of-plane vibrations of S are denoted by A_{1g}. When the number of layers increases from mono to bulk, a shift in both vibrations is observed. E_{2g}¹ undergoes the redshift, whereas A_{1g} inversely undergoes a blue shift. The shift in the value of E_{2g}¹ shows that a change in the thickness/

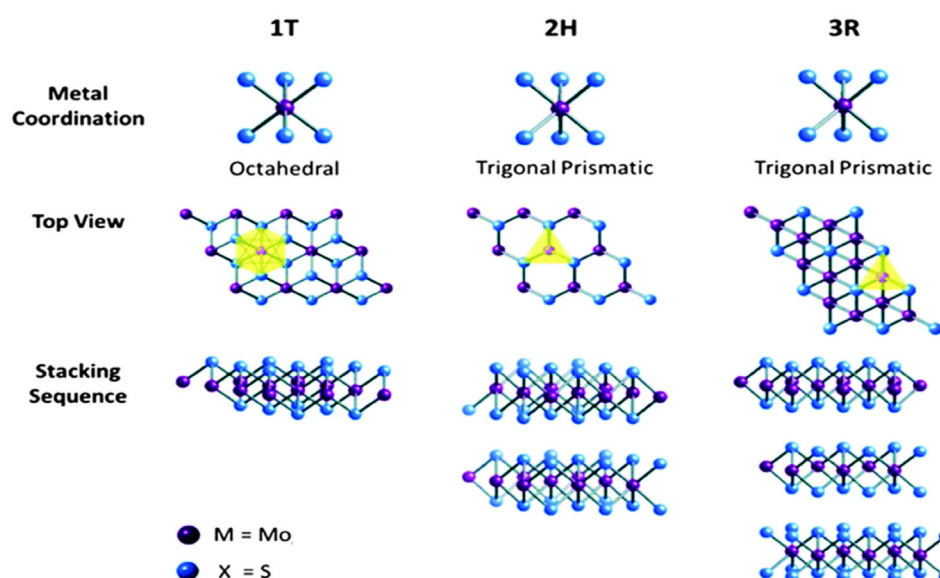


Fig. 1. 1T, 2H, and 3R phases of MoS₂. This was reproduced with permission from Ref. [19], Copyright (2017), The Royal Society of Chemistry.

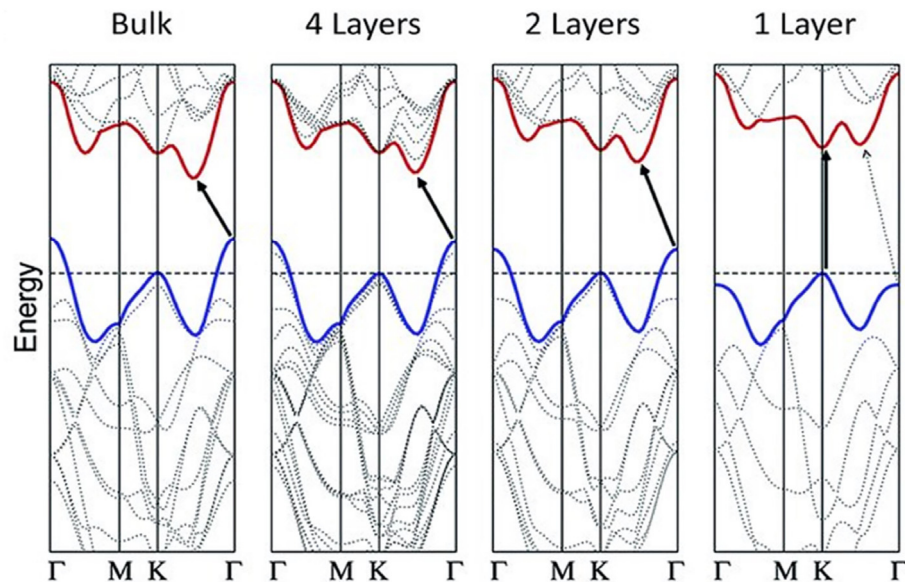


Fig. 2. Energy dispersion observed in bulk, 4-layer, 2-layer, and 1-layer MoS₂. This was reproduced with permission from Ref. [22], Copyright (2013), Macmillan Publishers Limited.

number of layers of MoS₂ induces a change in the bonding between adjacent layers [34]. The frequency difference between these two modes can be used as a convenient method to analyze the layer thickness of prepared MoS₂ samples.

The change in the type of bandgap helps in displaying an enhanced luminescence behavior in MoS₂. The photoluminescence (PL) of MoS₂ is inversely proportional to the thickness of the material, a characterization that is used in calculating the number of layers. Fig. 3 B shows that the intensity of two peaks at 670 nm and 627 nm is reduced while increasing the thickness from 1.3 nm to 7.6 nm [35]. These peaks are denoted as A1 and B1 excitons. The prominence of excitons shows the direct excitonic transition at point K, owing to the direct bandgap formed at lower thickness. The low PL intensity showed by bulk MoS₂ is due to the weak phonon interaction and strong excitonic absorption, which is bigger than its indirect bandgap [9]. This unusual behavior can be attributed to the quantum confinement of the electrons in d orbitals. Raman and PL showed similar trends in the behavior while moving from bulk to monolayer MoS₂.

3. Synthesis protocols of 2D MoS₂

The selection of an effective fabrication technique is necessary to enhance the desired properties of the synthesized MoS₂. The synthesis techniques can be divided into two main approaches, namely, top-down and bottom-up approaches. The top-down approach involves exfoliation techniques such as mechanical exfoliation, liquid-phase exfoliation, chemical intercalations, etc., whereas the bottom-up approach includes chemical vapor deposition (CVD) and chemical synthesis.

3.1. Exfoliation methods

With the advent of graphene synthesis using the 'scotch tape' method, mechanical exfoliation has been considered as one of the simplest methods for 2D material synthesis [36]. Bulk MoS₂ is peeled off using a tape and is rubbed against a substrate, which is mostly Si/SiO₂. A number of flakes of the bulk get attached to the substrate, whereas the van der Waals force between the layers

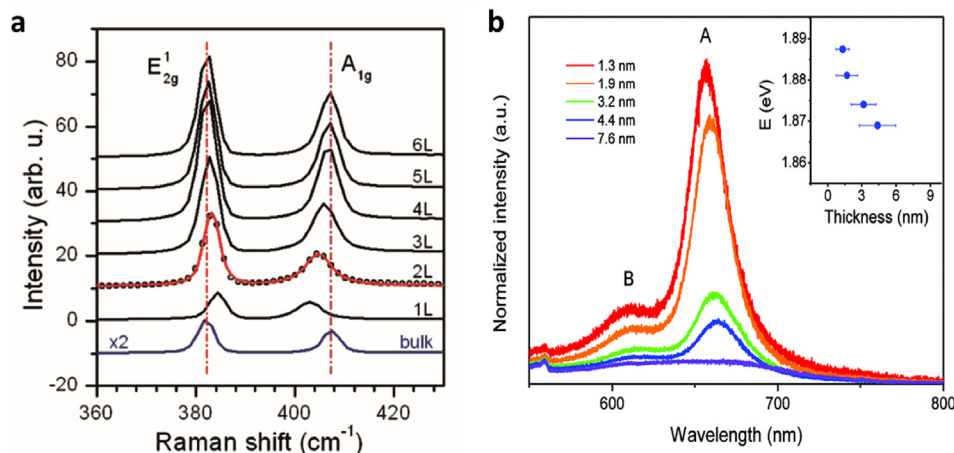


Fig. 3. (a) Raman spectra for 'n' layer (n = 1–6) and bulk MoS₂. This was reproduced with permission from Ref. [34], Copyright (2010), American chemical society. (b) Photoluminescence spectra of layered and bulk MoS₂. This was reproduced with permission from Ref. [35], Copyright (2011), American Chemical Society.

would further prevent few flakes from attaching to the substrate [37–39]. Hence, high-quality 2D MoS₂ sheets were obtained using the mechanical cleavage method, maintaining any intrinsic properties of MoS₂. However, low yield and uncontrolled sheet size, shape, and layer numbers prevent the practical application of this method [40].

An alternative class of exfoliation technique, the chemical exfoliation, namely, solvent based and ion intercalation based, has been reported [41]. Chemical exfoliation can be used for several structural modifications, doping different species, and the mass production of high-quality and uniform sized MoS₂ [42]. The choice of solvent and solute concentration play an important role in determining the thickness of the nanosheets generated. Organic solvents, such as *N*-methyl pyrrolidone (NMP), dimethylformamide, ethanol, isopropanol, etc., have been used to generate a high yield of MoS₂ nanosheets [43]. The selection of solvents depends on several parameters such as surface tension and Hildebrand and Hansen solubility parameters, where the Hildebrand parameter refers to a numerical estimate of the degree of interaction between the materials indicating the miscibility [41,44]. Exfoliation was found to be highly effective when the surface tension of the solvent matches well with that of MoS₂. Furthermore, controlling sonication time could result in an optimized flake size and concentration [45]. The effect of operating conditions on the synthesis of MoS₂ has been effectively studied using NMP as the solvent and a high-speed dispersive homogenizer as the shear device [46]. A yield of 4.3% of MoS₂ with a lateral size of 50–200 nm was obtained, which was found to be higher than most other shear exfoliation methods reported. However, prolonged sonication might cause defects in lattice structures which would reduce its efficiency in industrial applications, especially in circuits and other electronic devices [47].

Atomic intercalation is one of the top exfoliation methods to synthesize MoS₂ nanosheets. Intercalation involves the insertion of guest ion species into the host layered TMDCs, which weakens the van der Waals force of interaction between the two adjacent layers [48,49]. Alkali metal ions, such as Li⁺, K⁺, Na⁺, etc., are the commonly used species for intercalating in the host layers of MoS₂. Chemical intercalation and electrochemical intercalation are the two main categories of intercalation in fabricating TMDs [41]. Fig. 4 represents the schematics of both chemical and electrochemical intercalation.

n-Butyl lithium is the most common agent used for Li⁺ intercalation, hence exfoliating and producing 2D MoS₂ [50]. Electrochemical intercalation on the other hand occurs when an anode is discharged in a metal ion battery [51,52]. Bulk MoS₂ is used as the cathode, and the amount of lithium ions intercalated can be controlled by adjusting the discharge rate [15]. High yields of metallic 1T-MoS₂ can be fabricated through this technique which opens wide doors for exploiting novel applications.

3.2. Bottom-up approach

3.2.1. Thermal synthesis

Hydrothermal or solvothermal synthesis is one of the simplest and easily controllable techniques to develop 2D nanomaterials. In this, the sample is directly precipitated from the solution under high temperature and pressure, allowing the formation of different phases of MoS₂. Controlled morphology, aging, size of the particles, and uniformity are the main advantages of this synthesis route. MoS₂ nanosheets of varied sheet thickness and defects were synthesized via a controlled hydrothermal technique, producing MoS₂ with different morphologies, sulfur concentration, and surface area [53]. MoO₃, (NH₄)₆Mo₇O₂₄, and Na₂MoO₄ are the commonly used precursors for Mo, whereas elemental sulfur, KSCN, NH₂CSNH₂, Na₂S₂O₃, and thioacetamide are the common sulfur precursors used. Depending on the temperature used in the synthesis, different phases of MoS₂ such as 2H or 3R could be fabricated depending on the applications required [54].

The hydrothermal synthesis of flower-like MoS₂ was reported using hexaammonium heptamolybdate tetrahydrate ((NH₄)₆Mo₇O₂₄·4H₂O) and thiourea as precursors [55]. The reaction was performed in an autoclave for 12 h at 200 °C. The thiourea was responsible for reducing molybdenum from Mo⁶⁺ to Mo⁴⁺, and thiourea acted as a stabilizer for the nanosheet morphology. X-ray diffraction (XRD) pattern and the morphology of the synthesized flower-like MoS₂ and the comparison with the commercial MoS₂ sample are given in Fig. 5.

3.2.2. Chemical vapor deposition (CVD)

CVD has emerged as one of the best techniques to fabricate TMDs with sufficient crystal quality, tuneable size, thickness, and excellent electronic properties [56]. In a typical CVD technique, the

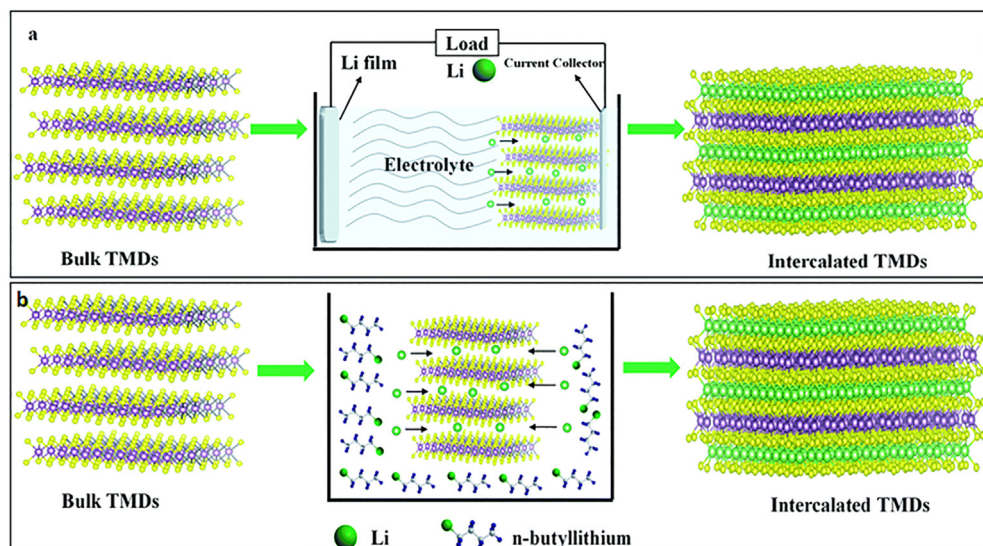


Fig. 4. Schematic of (a) electrochemical intercalation using metal ions (Li⁺) and (b) chemical intercalation followed by sonication or heating. This was reproduced with permission from Ref. [41], Copyright (2020), The Royal Society of Chemistry.

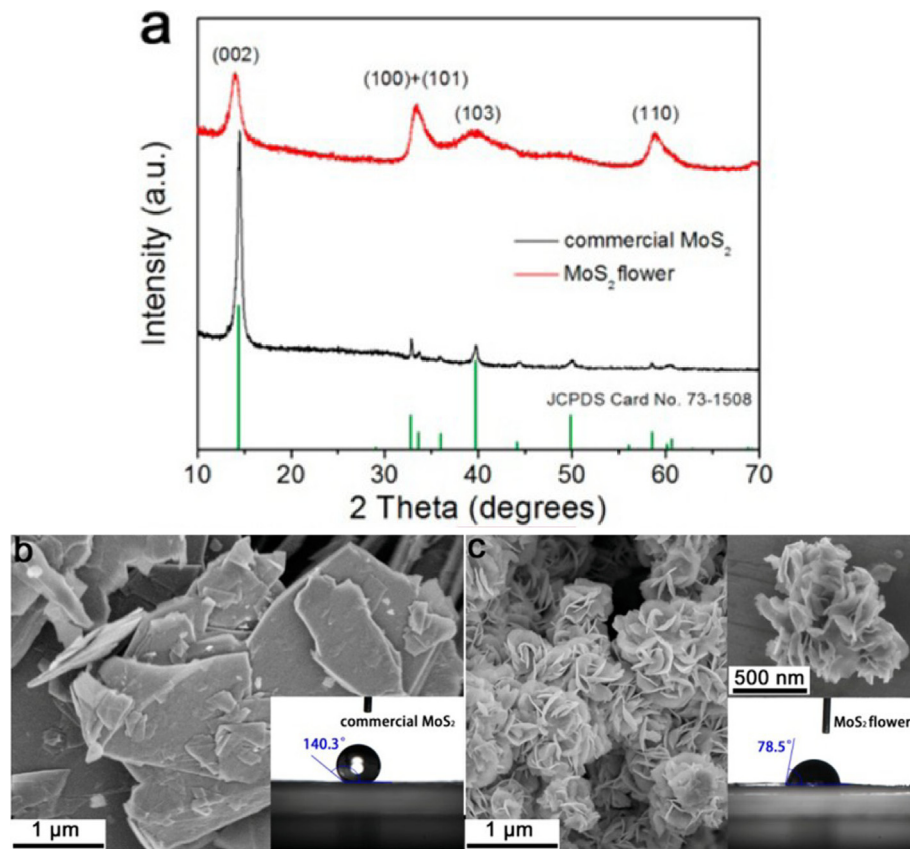


Fig. 5. (a) XRD pattern and (b&c) SEM images of the flower-like MoS₂ and commercial MoS₂ samples. This was reproduced with permission from Ref. [55], Copyright (2017), American Chemical Society.

solid precursors are heated under high temperature, which further forms a film on the substrate, mostly Si/SiO₂ wafers [47]. MoO₃ powder, S powder, vaporized S, or H₂S have been used as the most common precursors of Mo and S [57]. However, it was observed that using MoCl₅ as the solid precursor on different substrates produced MoS₂ with high surface area and offered an increased density of active sites, and reduced the electrical loss contact between the substrate and MoS₂ [58,59]. The normal heating temperature for CVD lies in the range of 700–1000 °C, which can be reduced to 150–300 °C under plasma-enhanced conditions [60]. Fig. 6a represents the cross section of a three-zone CVD growth chamber reported for the fabrication of monolayer MoS₂ [61]. As the vaporization of sulfur increases, it reacts with MoO₃ and results in the formation of MoO_{3-x}. The nitrogen carrier gas carries the MoO_{3-x} forward and reacts with the sulfur to form the MoS₂ molecules (Fig. 6c).

The impact of substrate types on the properties of CVD-grown MoS₂ has been studied by Strupinski et al. [62]. Three different substrates (SiO₂, graphene, and sapphire) were used to fabricate MoS₂. The graphene substrate showed only the formation of triangular domains as well as negligible change in the growth pattern of MoS₂ even under different growth conditions. SiO₂ yielded different morphologies, and the difference between the MoS₂ on both could be attributed to the variations in surface diffusion mechanisms on SiO₂ and graphene. It was concluded that graphene produces more uniform MoS₂ and hence is favorable for industrial-scale applications.

Recently, a potassium-assisted CVD technique was used for the phase selective synthesis of 1T' MoS₂ monolayers and 1T'/2H

heterophase bilayers [63]. This selective formation of 1T' phase MoS₂ was attributed to the lowering of the formation energy assisted by potassium. Fig. 7 represents the synthesis strategy adopted for tuning the relative stability of 2H and 1T' phases. As the potassium concentration exceeds 44%, the formation of the 1T' phase becomes feasible than the 2H phase. Studies revealed that the obtained MoS₂ acts as an ultrathin conductor, which further opens the door toward selectively designing high-quality 1T' MoS₂ for exploring wider applications.

4. Photoelectrochemical studies on MoS₂

Photoelectrochemical (PEC) studies using various photoanodes, such as TiO₂, TMDCs, etc., have drawn immense attention in the fields of energy, environment as well as health-related applications [64–68]. In a PEC cell, the solar energy is converted to hydrogen energy via an external bias applied to a photovoltaic material immersed in an electrolyte solution [69–71]. The semiconductor photoelectrodes can absorb the photons when exposed to light, acting as a photocatalyst. The fermi level (E_f) of the semiconductor is equilibrated with the redox potential of the solution via electron transfer. In case of an *n*-type semiconductor, the excited electrons will migrate toward the counter electrode, where the hydrogen generation takes place by the reduction of the electron acceptor generated by the photoanode [72]. The holes generated in the photoanode then undergo oxidative reactions, generating oxygen [73]. On the other hand, the *p*-type semiconductors act as photocathodes in water splitting reactions. The external bias applied helps in overcoming the additional voltage and slow kinetics of the

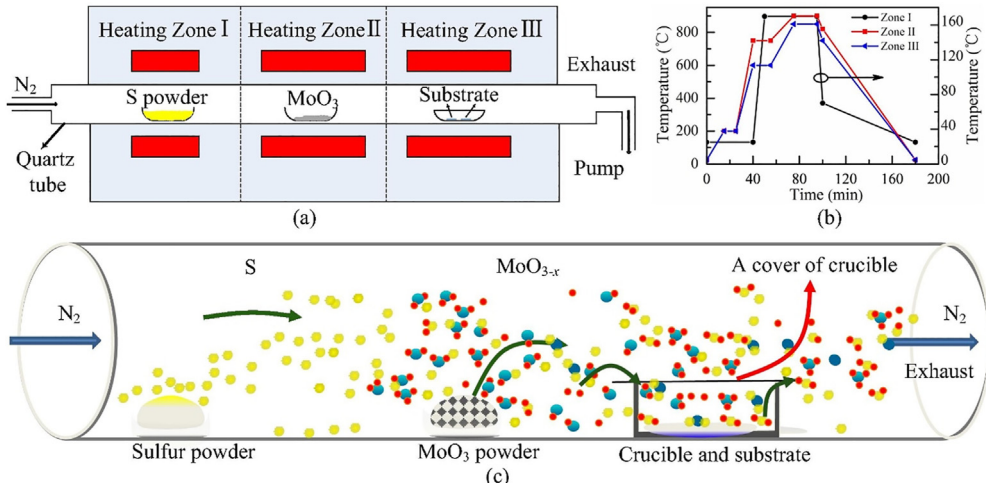


Fig. 6. (a) A diagrammatic representation of the three-zone CVD growth chamber. (b) Temperature program used for the synthesis of monolayer MoS₂. (c) Schematic illustration showing the growth of MoS₂ over the sapphire substrate. This was reproduced with permission from Ref. [61], Copyright (2017), Elsevier.

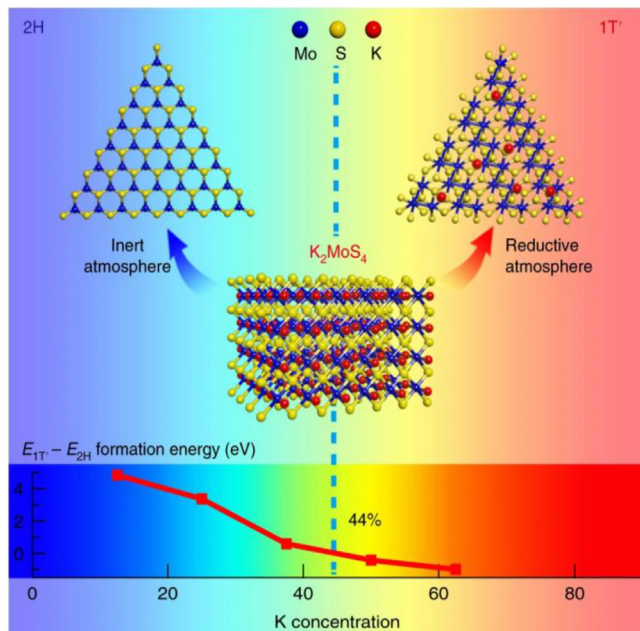
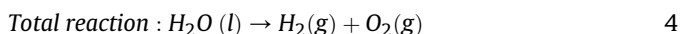
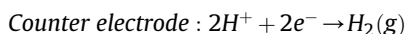
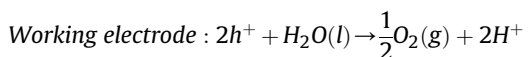


Fig. 7. Schematic illustration showing the phase-selective synthesis strategy of MoS₂ under reductive and inert atmospheres. The difference in the formation energy of both the phases of MoS₂ as a function of potassium concentration is shown at the bottom of the figure. This was reproduced with permission from Ref. [63], Copyright (2018), Nature Publishing Group.

water splitting reaction. The basic reactions involved in PEC water splitting are described as follows [72]:



where h and ν represent Planck's constant and the frequency of illuminated light, respectively. The major parameter used to

determine the efficiency of PEC water splitting is solar-to-hydrogen (STH) [53] conversion efficiency, which is given by:

$$STH = \frac{\text{Output energy as } H_2}{\text{Energy of incident solar light}} = \frac{rH_2 \times \Delta G}{P_{\text{sun}} \times S'} \quad 5$$

where ΔG is the gain in Gibbs energy, rH_2 is the rate of hydrogen production, P_{sun} is the energy flux of the sunlight, and S' is the area of the reactor [70].

MoS₂ is one of the commonly used TMDs for PEC water splitting reactions owing to its high PL quantum yield, availability of catalytic active edges, and stable hydrogen evolution reaction (HER) activity even under low pH conditions [74,75]. Investigations on the influence of the number of MoS₂ layers demonstrated that the chemically exfoliated monolayer MoS₂ produced the highest photocurrent [76]. This can be attributed to the reduced charge carrier mobility in multiple layers which further prevents the transport of charges effectively. However, fabricating single-layer MoS₂ is limited by the high temperature conditions, long reaction time, and limited control over the reaction conditions. Hence, several strategies, including doping, compositing, etc., have been used to improve the photocatalytic activity, conductivity, and thus the overall efficiency of PEC water splitting [77].

Constructing heterojunctions with other TMDCs, CdS, TiO₂, ZnO, graphene oxide (GO), g-C₃N₄, etc. has gained much attention in improving the efficiency of PEC activity of MoS₂ [79,80]. Mattevi et al. fabricated a MoS₂/WS₂ type II heterojunction via the CVD technique, demonstrating that the large flake size (100 μm) could reduce the charge carrier recombination rate compared with liquid phase exfoliated samples [81]. The MoS₂-coated Si nanowire (NW) hybrid was fabricated, wherein MoS₂ acted as a protection for SiNWs as well as improved the number of active sites for HER. The heterostructure exhibited a solar-to-hydrogen (STH) efficiency of 1.05% and a high durability of over 5 h [82]. Recently, a triple heterojunction of TiO₂/CdS/MoS₂ has been fabricated, and the influence of MoS₂ nanosheets on the heterojunction has been systematically investigated [78]. In this heterojunction, MoS₂ acts as a hole capturer, improving the hole transfer into the electrolyte solution, whereas CdS and TiO₂ help in harvesting a wide range of spectrum and improving the electrical conductivity, respectively. An increased photocurrent density of 3.25 mA/cm² at 0.9 V vs. Ag/AgCl was observed and was attributed to the accelerated charge transfer between the electrolyte and photoelectrode, caused by the

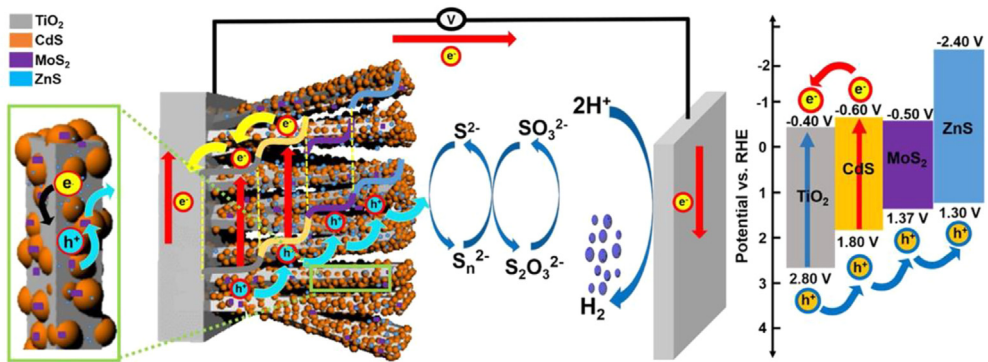


Fig. 8. Schematic representation of the charge transport mechanism in the $\text{TiO}_2/\text{CdS}/\text{MoS}_2$ photoanode. This was reproduced with permission from Ref. [78], Copyright (2019), Elsevier.

presence of MoS_2 nanosheets. Fig. 8 represents the schematic illustration of the charge transport mechanism in a $\text{TiO}_2/\text{CdS}/\text{MoS}_2$ photoanode. Ultrathin layer nature, improved chemical and physical stability, surface area, and accelerated electron mobility of MoS_2 aided in an improved PEC performance. However, additional research is required to improve the PEC activity of 2D TMDCs.

5. Photocatalytic hydrogen production using MoS_2

Hydrogen generation from water splitting using light is a sustainable way to address the rising demands of the hydrogen economy [84–87]. Nevertheless, splitting of water to produce hydrogen requires a higher enthalpy of 237 kJ/mol; it is an uphill reaction [88–90]. By using a suitable catalyst in the reaction, the energy expenditure can be decreased. In the photocatalytic hydrogen generation, the oxidation and reduction reactions simultaneously undergo on the catalyst surface as can be seen in Fig. 9. The photocatalytic water splitting reaction mechanism is well known [91–94]. During the photocatalytic process, when the potential of the electron-hole pairs formed in the conduction band minimum (CBM) and valence band maximum (VBM) is more negative and positive than the redox potential of H^+/H_2 , they migrate to the surface of the photocatalyst to react with water in the surface-active sites. The electrons will reduce the water to hydrogen, while the holes get oxidized to form oxygen simultaneously. For enhancing the photocatalytic efficiency of the system, a promoter like cocatalysts is added in the reaction as shown in Fig. 9b.

The cocatalyst acts as a support catalyst to accelerate the reaction by capturing the excited electrons to diminish the photo-generated charge recombination. Noble metals such as Pt, Pd, Au, and Ag are used as cocatalysts for photocatalytic water splitting reactions [95–99]. However, availability and cost restrict its use in high scalable hydrogen production applications. Therefore, 2D materials such as MoS_2 have been used to substitute these noble metals in photocatalysis because of their high conductivity and enhanced hydrogen production activity. The 2D layers in MoS_2 increase the electron conductivity and act as an activation site for the reduction reaction.

Recently, Liu et al. demonstrated the hydrothermal synthesis of mixed-phase MoS_2 layers coated on TiO_2 nanorod arrays ($\text{MoS}_2@\text{TiO}_2$ NRs) [100]. The rationale behind the design was to use the synergistic effect of two polymorphs of MoS_2 (2H and 1T) to enhance the charge separation. In $\text{MoS}_2@\text{TiO}_2$ NRs, the 2H (semiconducting phase) formed a heterojunction with TiO_2 , whereas the 1T (metallic phase) acts as the

cocatalyst during the reaction. The MoS_2 sheets were uniformly grown on the TiO_2 rods and were controlled by varying reaction times. The incorporation of MoS_2 sheets increased the hydrogen production rate by providing active edges for H_2 evolution. $\text{MoS}_2@\text{TiO}_2$ NRs exhibited an evolution rate of $8.43 \mu\text{mol}/\text{cm}^2/\text{h}$, which is 13 times higher than the TiO_2 parent sample. The photocurrent studies observed that the mixed-phase 1T/2H MoS_2 showed prominently metallic character, as the electrons readily transferred from TiO_2 to MoS_2 and then transferred to the electrolyte. This characteristic behavior is explained by the intercalation of energy bands of 2H and 1T in the MoS_2 layer, which gives rise to a continuous energy band across the Fermi level as in metals.

A novel photocatalyst that can be used without a sacrificial agent was reported by Li et al. (Fig. 10a). They developed a 2D composite structure of Ru-doped single-layer MoS_2 supported by polar cerium nanocrystals (Ru: SL- $\text{MoS}_2/\text{CeO}_2$ NCs) [28]. Polar surface material (CeO_2 (100)) has a net dipole moment acting perpendicular to the surface [101]. The catalyst showed stable oxygen and hydrogen production until 10 h of irradiation (Fig. 10b). The quantum efficiency (QE) of the system was tested by varying the wavelengths from the UV region to the visible region (Fig. 10c). The highest QE was obtained at the UV region (385 nm), and as the wavelength increased, QE was observed to decrease, which was likely due to the sudden decrease in photon absorption [102]. CeO_2 (100) nanocube-supported Ru: SL- MoS_2 showed three times enhanced hydrogen activity (2977 mmol/h/g) than the parent sample Ru: SL- MoS_2 (821 mmol/h/g). The high QE of 2D MoS_2 with the polar-faceted cerium support is due to the strong charge separation due to polarization induced by CeO_2 NCs. Thus, it extends the exciton lifetime of 2D MoS_2 .

In a recent study, lamellar flower-like MoS_2 was reported as a cocatalyst to improve the hydrogen evolution efficiency of CdS [103]. The heterojunction formation between the CdS nanoparticles and lamellar MoS_2 accelerated the photoinduced electron transfer. The MoS_2/CdS system achieved 36 times hydrogen evolution activity compared with the pure CdS . The maximum hydrogen evolution (54.1 mmol/h/g) was observed for the 30% MoS_2 -incorporated MoS_2/CdS composite (Fig. 11a). The UV-diffuse reflectance spectroscopy (UV-DRS) (Fig. 11b) shed insights on the enhanced hydrogen evolution performance of the 30% MoS_2/CdS catalyst. The incorporation of MoS_2 in CdS decreased the bandgap from 2.25 eV (pure CdS) to 2.08 eV (30% MoS_2/CdS). The narrow bandgap represents the broader light absorption range and that in turn leads to the higher photocatalytic activity.

Different techniques such as doping, nanostructuring, and heterojunction formation with other semiconductors have been used

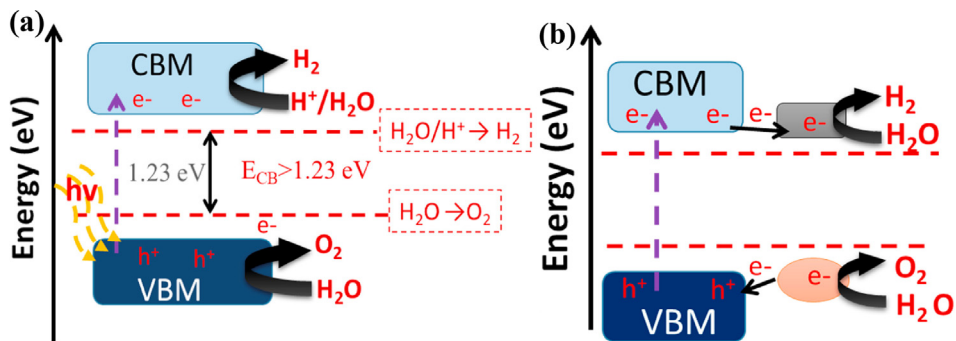


Fig. 9. Schematic diagram of photocatalytic water splitting. (a) Full photocatalytic reaction, (b) with the addition of the cocatalyst. This was reproduced with permission from Ref. [83], Copyright (2017), Elsevier.

to tune the properties of MoS_2 to improve photocatalytic hydrogen production. Recent studies on MoS_2 composites for photocatalytic hydrogen production are summarized in Table 1.

6. Treatment of organic pollutants

6.1. Mechanism of photocatalytic degradation of contaminants by MoS_2

MoS_2 with a bandgap in the visible range has been applied for the photocatalytic degradation of several dyes, antibiotics, and other contaminants of emerging concern [13,113–115]. The crystal structure, surface chemical modification, and number and thickness of MoS_2 layers are the key parameters determining the photocatalytic activity of MoS_2 [114]. Generally, the photocatalytic degradation reaction utilizes the electron transfer from the highly reactive radical species to the contaminant molecules and chops down the hazardous contaminants into small molecules. The key reactive species involves the holes (h^+), hydroxyl radicals, and superoxide radicals ($\cdot\text{O}_2^-$) [13]. A schematic representation of the photocatalytic electron transfer

process in 2D MoS_2 -based material leading to the degradation of contaminants is summarized in Fig. 12. To better understand the role of specific reactive species in the reaction, several scavengers are used. Isopropanol is used as a scavenger for hydroxyl radicals, and benzoquinone and ammonium oxalate scavenge the $\cdot\text{O}_2^-$ and h^+ , respectively [11]. Calculating the VB and CB potentials of the synthesized catalyst is crucial in elucidating the mechanism of electron transfer processes in a photocatalytic reaction [116].

6.2. MoS_2 material as a catalyst for degradation of contaminants

In its natural form, MoS_2 is found in the 2H (hexagonal) form [117]. However, because a high electron carrier concentration is found in 1T MoS_2 [118], the transformation from 2H to 1T MoS_2 is beneficial for photocatalytic applications. Xia et al. obtained 1T MoS_2 from the hydrothermally synthesized 2H phase by Li intercalation. In the study, 1T MoS_2 with Au nanoparticles showed up to 90.4% decomposition for methylene blue in 20 min, which was only 25.2% for the case of 2H– MoS_2 [118]. Saha et al. [119] studied the MoS_2 -polyaniline (PANI) nanocomposite fabricated by *in situ*

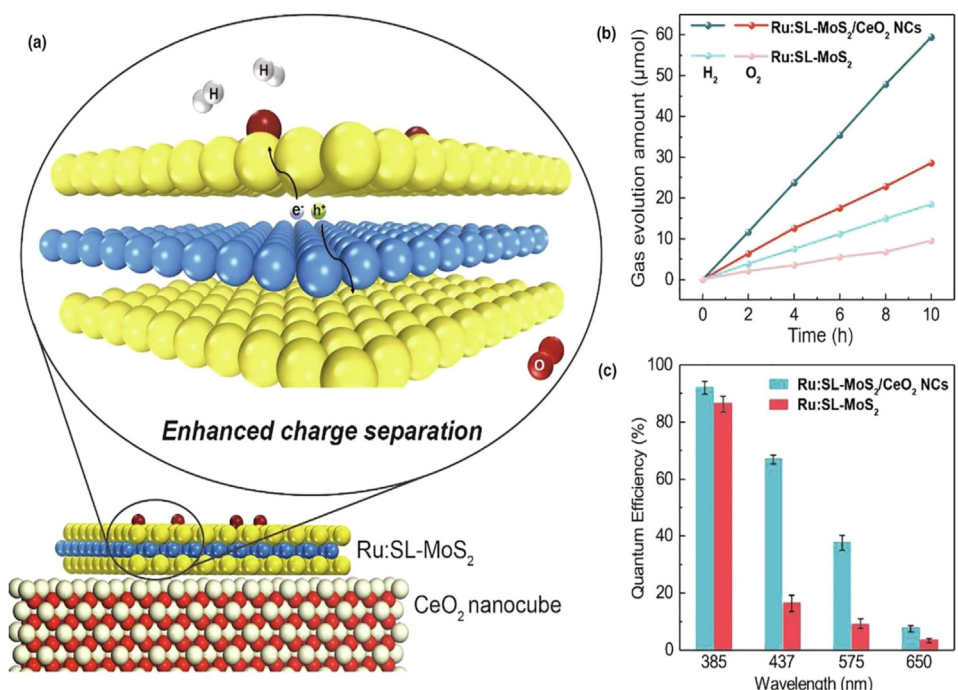


Fig. 10. (a) Schematic diagram of Ru: SL-MoS₂/CeO₂ NCs. (b) Evolution of O₂ and H₂ by photocatalytic water splitting and (c) the quantum efficiency of Ru: SL-MoS₂/CeO₂ NCs and Ru: SL-MoS₂. This was reproduced with permission from Ref. [28], Copyright (2020), Elsevier.

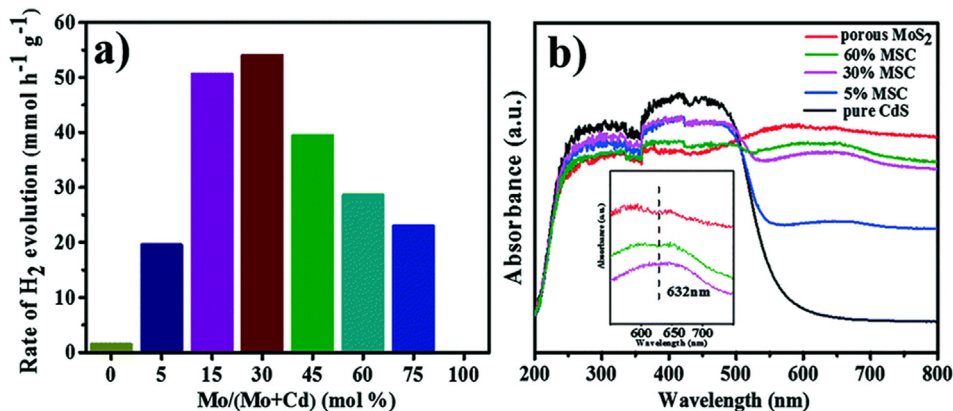


Fig. 11. (a) Comparison of hydrogen evolution activity of the MoS₂/CdS catalyst by varying the mol% of MoS₂. (b)UV-DRS spectra of the various MoS₂/CdS composites. This was reproduced with permission from Ref. [103], Copyright (2021), The Royal Society of Chemistry.

polymerization for the degradation of methylene blue and 4-chlorophenol (4-CP). The intercalation of PANI into MoS₂ reduced the agglomeration between the nanosheets and enhanced the electronic conductivity. The composite showed 30% methylene blue degradation in less than 3 h and 75% degradation for 4-CP in 1 h. In another study by Quinn et al. [120], MoS₂ suspension in Milli-Q filtered water was used to degrade methylene blue (MB) and resulted in degradation of 90% of the original concentration after 2 h. Li et al. [121] adopted a hydrothermal method to synthesize flower-like MoS₂, and nanoparticles with varying sheet thickness were obtained by adding polyethylene glycol (PEG) with varying molecular weights as additives. Observations showed that increasing molecular weight of PEG led to a decrement in sheet thickness which adversely affected the photocatalytic performance. The degradation rate for MB was observed to decrease from 64.2% to 11.2% when the sheet thickness varied from 23 nm to 13 nm for PEG200 and PEG8000.

6.3. MoS₂/TiO₂ composites for contaminant degradation

Instead of a single photocatalyst like MoS₂ or TiO₂, composite photocatalysts show higher photocatalytic activity [122]. Hu et al. [123] adopted a two-step hydrothermal method to synthesize a 3D double-heterostructured photocatalyst with MoS₂–TiO₂ core-shell nanosheets assembled on a graphite fiber. The structure showed highly efficient electron-hole generation and enhanced carrier separation. For methyl orange dye, the structure showed 88% and 90% degradation under exposure of UV and visible light, respectively, for 30 min, which was significantly higher than GF@TiO₂ (55% for UV irradiation). Liu et al. [124] created a sandwich-like 3D mesoporous composite TiO₂/MoS₂/TiO₂ nanosheet structure which showed up to 89.86% degradation of methylene blue within 120 min of irradiation by visible light. Another 3D hierarchical configuration formed by the hydrothermal method in the

study of Zhou et al. [104] was based on MoS₂ nanosheets coated on a TiO₂ nanobelt. The TiO₂ nanobelt inhibited the growth of MoS₂ crystals along the *c*-axis, resulting in a nanobelt with a coating of only a few layers. This structure resulted in complete degradation of rhodamine-B in 20 min, whereas the degradation by pure TiO₂ and MoS₂ was 35.3% and 86.9%, respectively, under the same conditions. Another TiO₂/g-C₃N₄/MoS₂ composite obtained by the liquid exfoliation and solvothermal process was developed by Zhang et al. [122]. In the photocatalytic degradation experiment of methyl orange, the synthesized composite showed better photocatalytic activity than TiO₂, pure g-C₃N₄, and TiO₂/g-C₃N₄. The enhanced activity was attributed to the efficient utilization of photons and enlarged spectral response owing to the heterostructure between the g-C₃N₄/MoS₂ hybrid and TiO₂ nanostructure.

6.4. Self-cleaning properties of MoS₂

Similar to surfaces based on TiO₂, MoS₂ shows excellent self-cleaning properties [125]. However, unlike TiO₂, the antifouling and self-cleaning properties of MoS₂ have not yet been widely studied. Many organic dyes, industrial chemicals, and agricultural wastes impose risks to the environment, and their elimination by various means becomes necessary [113,126,127]. At the same time, the continuous operation of the photocatalytic system requires a clean surface for further adsorption of contaminants to ensure their photocatalytic degradation.

Owing to its high photocatalytic capability, strong absorption of visible light, and low cost, MoS₂ has emerged as an excellent candidate as a photocatalyst or co-photocatalyst for decontamination of various organic pollutants [113]. MoS₂ shows extremely low friction surface and low roughness which are suitable in preventing the development of fouling [128]. The phenomenon of self-cleaning on a surface generally refers to contaminant removal by either

Table 1

Hydrogen evolution studies of different MoS₂-based systems in photocatalytic water splitting.

Photocatalyst used	Light source	Sacrificial agent used	Activity	Ref.
TiO ₂ @MoS ₂	300 W Xe arc lamp	0.35 M Na ₂ S and 0.25 M Na ₂ SO ₃	6 mmol/h/g	[104]
2D MoS ₂ /CdS p-n nanohybrids	300 W Xe lamp	10 vol% lactic acid	137 μmol/h	[105]
CdS–Au/MoS ₂	Xe lamp	10 vol% lactic acid	7 mmol/h/g	[106]
CeO ₂ @MoS ₂ /g-C ₃ N ₄	3 W UV-LEDs	0.5 M Na ₂ S and 0.5 M Na ₂ SO ₃	65.4 μmol/h	[107]
Phosphated-MoS ₂ /NiTiO ₃	5 W LED incandescent lamp	15 vol% triethanolamine	67.6 μmol/h	[108]
1T-MoS ₂ /g-C ₃ N ₄	300 W Xe lamp	20 vol% triethanolamine	4426 μmol/h/g	[109]
8%MoS ₂ @Zn _{0.5} Cd _{0.5} S	300 W Xe lamp	Amoxicillin solution	630 μmmol/h	[110]
P-doped MoS ₂	300 W Xe lamp	0.2 M Na ₂ SO ₃ and 0.2 M Na ₂ S	975.7 mmol/h/g	[111]
Ru: MoS ₂ /CeO ₂ NCs	70 W tungsten light	No sacrificial agent	2977 mmol/h/g	[28]
Lamellar porous MoS ₂ /CdS	300 W Xe lamp	10 vol% lactic acid	54.1 mmol/h/g	[103]
S-doped g-C ₃ N ₄ /N-doped MoS ₂	300 W Xe lamp	10 vol% triethanolamine	658.5 μmol/h/g	[112]

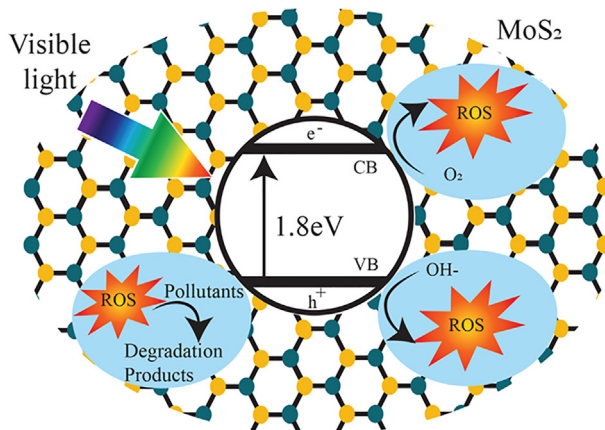


Fig. 12. Illustration of the various steps involved in the electron transfer processes in the 2D MoS₂, leading to the degradation of contaminant molecules.

highly mobile droplets on a hydrophobic surface (contact angle $>90^\circ$) or by a sweeping action by spreading liquid on a hydrophilic surface (contact angle $<90^\circ$) [129]. A higher mobility of liquid droplets is obtained on surfaces with increasing contact angles, and it is generally achieved by creating a surface roughness component on a hydrophobic surface [130,131].

The photocatalytic action of MoS₂ can assist the self-cleaning activity by decomposing the contaminants into harmless species which can be subsequently removed because of its hydrophobic nature. In conclusion, in the photocatalytic decontamination process, the electron transfer from highly active radical species breaks down the contaminant particles on the surface into harmless compounds under light illumination. Carbon-based materials such as GOs and reduced GOs (rGOs) are well known for their remarkable antifouling properties. However, MoS₂ nanosheets have been proven even better than GO and rGO in preventing the accumulation and growth of natural organic matter and *Escherichia coli* bacteria [132]. In various applications like removal of pharmaceutical wastes, MoS₂ has also been adopted as an adsorbent owing to $\pi-\pi$ stacking, its hydrophobic behavior, and electrostatic interactions [133]. This way, the high adsorbent capacity of MoS₂ also assists the subsequent photocatalytic removal of contaminants. In summary, a synergistic combination between the three phenomena (adsorption, degradation, and removal) imparts MoS₂ excellent self-cleaning properties under light irradiation.

2D MoS₂ layers when aligned vertically depict more chemical activity than horizontal 2D MoS₂ owing to multiple 2D edge sites due to their enriched dangling bonds. Furthermore, a thin coating with the Pt noble metal on pristine MoS₂ was proven to be effective in the degradation of harmful compounds like microcystin-LR produced by algal blooms under visible light [127]. The use of noble metals results in surface plasmon resonance, which significantly enhances the optical absorption. Where MoS₂ by itself shows high photocatalytic activity toward contaminant degradation, its use to form various composite structures has numerous additional benefits. For instance, hybridized composite photocatalysts show reduced bandgap and reduced recombination of electron-hole pairs, further enhancing the photocatalytic activity toward various organic and bio pollutants [127,134–136]. In addition, MoS₂ hybridization with graphene has shown to result in faster separation of charge carriers, ultimately leading to higher degradation rates of methylene blue [134,135].

The contaminant sweeping action for dust particles has been demonstrated on hydrophobic TiO₂/polyvinylidene fluoride (PVDF) @MoS₂ core-shell heterostructured composite fibers which can considerably reduce maintenance costs [137]. MoS₂ nanoparticles with cauliflower-like morphology were grown on TiO₂/PVDF flexible fibers by a single-step hydrothermal method. The surface showed contact angles high as 128.28°, 120.30°, and 129.27° for water, rhodamine-B, and methyl orange, respectively. Under visible illumination for 150 min, both the dyes lost their colors completely, showing an excellent degradation capability and self-cleaning against these two dyes. Similarly, hydrothermally developed MoS₂ ternary composite Pt/vertically aligned MoS₂/TiO₂ is found to be more effective than pristine TiO₂ nanotube array in degrading rhodamine 6G under visible light irradiation [125]. In many applications, crude oil spills impose limitations on the choice of absorbent materials owing to the high viscosity of crude oil. However, under simulated sunlight illumination, a MoS₂ sponge showed a rise in its temperature (from room temperature to 76 °C in 70 s) which led to the significant reduction in crude oil viscosity, ultimately increasing its absorption on the MoS₂ rubber sponge [138].

7. Photocatalytic disinfection

7.1. Mechanism of disinfection

Semiconducting photocatalysts create reactive oxygen species [48] to allow for the disinfection of water. To do this, their bandgap energy is excited by a photon that has higher energy than the

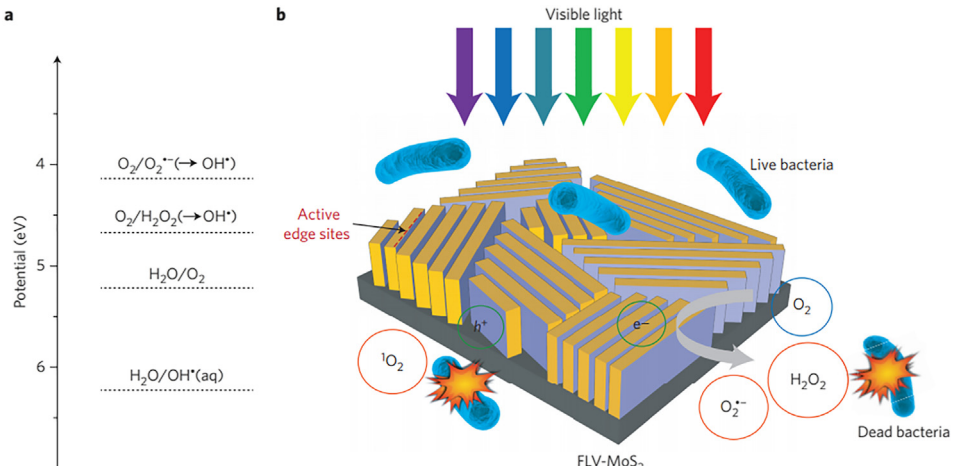


Fig. 13. Vertically layered MoS₂: (a) Depiction of the ROS-formation potential. (b) Inactivation of bacteria using MoS₂ due to the formation of ROS from visible light photocatalysis. This was reproduced with permission from Ref. [141], Copyright (2016), Macmillan Publishers Limited.

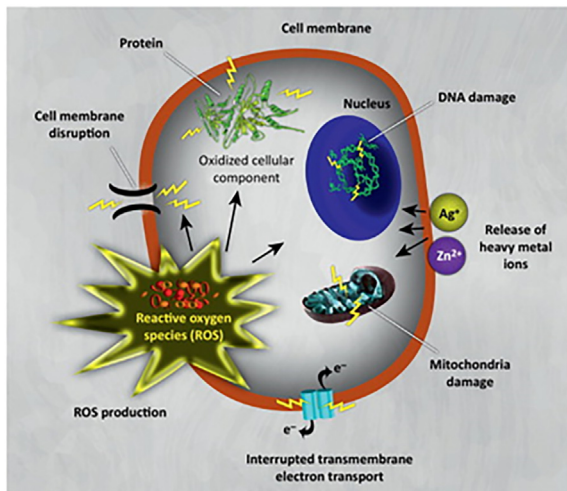


Fig. 14. Mechanisms of toxicity of MoS₂ against bacteria. This was reproduced with permission from Ref. [142], Copyright (2012), Elsevier.

bandgap. This causes electrons to be excited and to move from the VB to the CB. The holes left behind by the electrons and the newly excited electrons can react with the water and dissolved oxygen to form the reactive oxygen species (ROS) [126,139,140]. Fig. 13 illustrates the formation of these ROS and the potential (eV) for their formation.

These ROS cause oxidative stress to occur on the microorganisms, resulting in disinfection [142] (Fig. 14). The cell membrane of the microorganism breaks down allowing the photocatalyst to act internally, resulting in cell death [17,143,144]. Several theories have been proposed for the degradation of the bacteria such as the leakage of K⁺ and Ca²⁺ ions from the cell membrane [145]. The main method of photocatalytic disinfection is believed to be from lipid peroxidation [146]; this results in the inhibition of normal activities of the cell such as respiration [145].

7.2. Water treatment

MoS₂ consists of molybdenum atoms in a hexagonal plane linked to sulfur atoms that are hexagonally arranged. These layers

are held together by weak van der Waals forces [147]. When chemically exfoliated 2D MoS₂ sheets were compared with bulk MoS₂ powder in the elimination of *E. coli*, viability loss of 91.8% and 38.9%, respectively, was found. MoS₂ has been reported to be capable of rapid disinfection of water when several layers of MoS₂ are vertically aligned [148]. It was found that when positively charged MoS₂ had its hydrophobicity altered, the mechanism of disinfection could be changed to the membrane of the bacteria being depolarized rather than oxidative stress because of ROS generation.

By vertically aligning MoS₂ into films, it was possible to make use of the complete visible light spectrum and increase the bandgap from 1.3 to 1.55 eV. This method showed an increase of 15 times log efficiency of inactivation of bacteria in water [141]. MoS₂ can be modified to create a few layers of nanosheets or a single layer with ease. Its bandgap is 1.2 eV in bulk form, and this can be increased when formed into a monolayer structure [149]. This initial low bandgap and lack of active sites make bulk MoS₂ limited as a photocatalyst; however, this can be overcome when used as a cocatalyst. The use of MoS₂ and Fe₃O₄ to form a Fenton-like catalyst was capable of inactivating bacteria in a pH range between 3.5 and 9.5. This composite was capable of complete degradation of *E. coli* within 6 min when 5 mM H₂O₂ was added with a starting bacterial concentration of 1.2×10^6 CFU/ml [150]. The exposure of *E. coli* to 20 and 40 µg/ml of MoS₂ reduced bacteria presence by 70% and 84%, respectively. This decrease was also seen in *Staphylococcus aureus* with a decrease of 63% and 97% in 40 and 80 µg/ml, respectively [151]. The MoS₂/Ag₂CO₃ composite was capable of complete inactivation of *E. coli* using a 5% concentration within 80 min [152]. One study created a pyramid-like MoS₂ layered structure; this incorporated decreasing sized MoS₂ sheets going up the layers to form this pyramid-like shape (Fig. 15). This was capable of eliminating 99.99% of *E. coli* using simulated visible light after 40 min [153].

7.4. Inactivation of antibiotic-resistant organisms

2D-MoS₂ sheets were found to be capable of binding to the enzyme β-lactamase, inhibiting its functions. This inhibition was found to help prevent the growth of antibiotic-resistant organisms such as methicillin-resistant *S. aureus* [154]. By tuning the surface chemistry of the 2D-MoS₂, it is believed that enhanced inhibition could be developed. The MoS₂/α-NiMoO₄ composite was used for

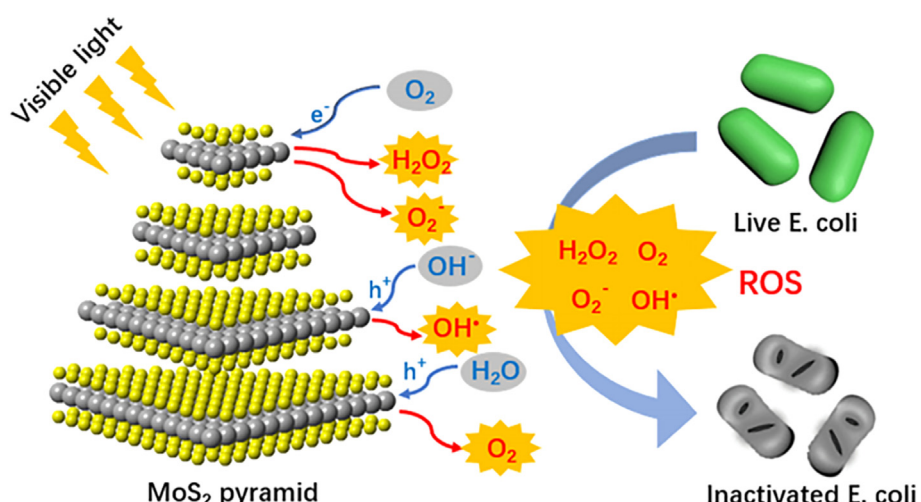


Fig. 15. Photocatalytic disinfection of *E. coli* using pyramid-shaped MoS₂ layers and visible light. This was reproduced with permission from Ref. [153], Copyright (2018), American Chemical Society.

the elimination of multidrug-resistant *S. aureus*, with complete inactivation obtained after 150 min using visible light. The inactivation was evident with the organism undergoing protein and DNA degradation, and damage was visible on the cell membrane [155]. rGO–MoS₂–Ag was used to disinfect antibiotic-resistant *S. aureus* and *E. coli*, where to inhibit their growth, concentrations of 100–200 µg/ml and 50–100 µg/ml were needed, respectively. This inhibition was believed to be a result of excellent ROS generation [156]. A Fe₂O₃@MoS₂ composite was found to be capable of preventing the conjugative transfer of antibiotic-resistant genes. A study showed that the composite could greatly inhibit the conjugation of the interference of RP4-7 plasmid [157]. A separate study using a Fe₂O₄@MoS₂ composite found it to be capable of preventing horizontal gene transfer, one of the main contributions to antibiotic resistance [158].

8. Challenges, strategies for improvement, and future directions

The limited number of active edge sites available for the photocatalytic reaction and the rapid recombination of electrons and holes are the major challenges associated with the practical application of 2D MoS₂ photocatalysts. The fast recombination of electron-hole pairs leads to lower QE and decreases the photocatalytic degradation capability of these materials. Doping MoS₂ with transition metal elements can generate defect positions and alter the crystallinity of MoS₂. Transition metal element doping of MoS₂ also improves the visible light absorption range of MoS₂. A zerovalent iron-doped g-C₃N₄–MoS₂ composite accelerated the electron-hole pair separation and resulted in efficient contaminant degradation [159]. The number of catalytic active sites could be enhanced by strategies such as doping and heterojunction formation. Heterojunction formation helps in the rapid separation of electron-hole pairs by acting as an ideal channel for the movement of charge carriers. In a recent study, the MoS₂/TiO₂ type II heterojunction catalyst has shown enhanced interfacial charge transfer and excellent photoelectrocatalytic hydrogen evolution capacity [160].

The poor recyclability of MoS₂-based catalysts is resolved by incorporating MoS₂ with Fenton (iron-based) catalytic systems. Magnetic properties associated with iron-based catalysts enhance the recyclability of MoS₂ photocatalysts. The MoS₂/rGO/Fe₃O₄ composite with flower-like morphology demonstrated a large potential for recyclability [161]. Different synthesis protocols are reported for the preparation of 2D MoS₂ catalysts via bottom-up and top-down approaches. However, further research is warranted for the cost-effective preparation of 2D-MoS₂ for industrial-scale applications.

The use of MoS₂-based systems for the photocatalytic reduction of CO₂ into value-added products is an emerging research area [65]. A recent study reported a TiO₂/2D MoS₂ nanostructure for the photocatalytic CO₂ reduction [162]. Similarly, a few layered MoS₂ in combination with graphene and TiO₂ demonstrated its potential for CO₂ reduction [163]. Hence, a bright future is wide open for the 2D MoS₂-based systems for energy and environmental applications.

9. Conclusions

2D MoS₂-based materials have been widely explored for applications in the areas of environmental remediation and energy shortage. The visible light absorption capacity of 2D MoS₂ makes it capable of maximum utilization of solar light, which is one of the cheapest sources of energy. The observed changes in the band structure of MoS₂, while moving from 3D to 2D, are dramatic. The number of layers associated in the material determines the physical and chemical properties of 2D MoS₂-based photocatalysts. In addition, various crystal phases observed in MoS₂ decide their

electronic properties and band structure. Among the various protocols used to synthesize 2D MoS₂, the solvothermal synthesis method helps to arrive at uniform particles with controlled morphology. The PEC water splitting reaction using MoS₂ is one of the emerging areas of research. The low cost of MoS₂ compared with the noble metals makes it the cheapest alternate to be explored for photocatalytic hydrogen production applications. The composite material of MoS₂ with TiO₂, g-C₃N₄, and the graphene family of materials has demonstrated excellent potential for contaminant degradation. Reactive oxygen species generated on light irradiation on MoS₂ create oxidative stress on microorganisms, and this property is utilized for water disinfection.

Difficulties in recycling the catalyst and the limited number of available active edge sites delimit the practical applications of MoS₂ photocatalysis. Hence, there is a lot of room for development in this research area, and intense research is required to utilize the 2D MoS₂-based materials for industrial-scale applications.

Declaration of competing interest

The authors declare that they have no known competing financial interests or personal relationships that could have appeared to influence the work reported in this paper.

Acknowledgements

PF and AG would like to acknowledge the support of the IT Sligo Presidents Bursary Scheme in this research.

References

- [1] N. Serpone, A.V. Emeline, Semiconductor photocatalysis — past, present, and future outlook, *J. Phys. Chem. Lett.* 3 (2012) 673–677.
- [2] M. Pelaez, N.T. Nolan, S.C. Pillai, M.K. Seery, P. Falaras, A.G. Kontos, P.S.M. Dunlop, J.W.J. Hamilton, J.A. Byrne, K. O'Shea, M.H. Entezari, D.D. Dionysiou, A review on the visible light active titanium dioxide photocatalysts for environmental applications, *Appl. Catal. B: Environ.* 125 (2012) 331–349.
- [3] B. Luo, G. Liu, L. Wang, Recent advances in 2D materials for photocatalysis, *Nanoscale* 8 (2016) 6904–6920.
- [4] L. Zhang, M. Jaroniec, Toward designing semiconductor-semiconductor heterojunctions for photocatalytic applications, *Appl. Surf. Sci.* 430 (2018) 2–17.
- [5] D.B. Sulas-Kern, E.M. Miller, J.L. Blackburn, Photoinduced charge transfer in transition metal dichalcogenide heterojunctions — towards next generation energy technologies, *Energy Environ. Sci.* 13 (2020) 2684–2740.
- [6] Q. Fu, J. Han, X. Wang, P. Xu, T. Yao, J. Zhong, W. Zhong, S. Liu, T. Gao, Z. Zhang, L. Xu, B. Song, 2D transition metal dichalcogenides: design, modulation, and challenges in electrocatalysis, *Adv. Mater.* (2020) 1907818.
- [7] S. Manzeli, D. Ovchinnikov, D. Pasquier, O.V. Yazyev, A. Kis, 2D transition metal dichalcogenides, *Nat. Rev. Mater.* 2 (2017) 17033.
- [8] Z. Wei, B. Li, C. Xia, Y. Cui, J. He, J.-B. Xia, J. Li, Various structures of 2D transition-metal dichalcogenides and their applications, *Small Methods* 2 (2018) 1800094.
- [9] A. Splendiani, L. Sun, Y. Zhang, T. Li, J. Kim, C.-Y. Chim, G. Galli, F. Wang, Emerging photoluminescence in monolayer MoS₂, *Nano Lett.* 10 (2010) 1271–1275.
- [10] K.F. Mak, C. Lee, J. Hone, J. Shan, T.F. Heinz, Atomically thin MoS₂: a new direct-gap semiconductor, *Phys. Rev. Lett.* 105 (2010) 136805.
- [11] Y. Yuan, R.-t. Guo, L.-f. Hong, X.-y. Ji, Z.-s. Li, Z.-d. Lin, W.-g. Pan, Recent advances and perspectives of MoS₂-based materials for photocatalytic dyes degradation: a review, *Colloid. Surface. A: Physicochem. Eng. Aspect.* 611 (2021) 125836.
- [12] B. Han, Y.H. Hu, MoS₂ as a co-catalyst for photocatalytic hydrogen production from water, *Energy Sci. Eng.* 4 (2016) 285–304.
- [13] M.-h. Wu, L. Li, N. Liu, D.-j. Wang, Y.-c. Xue, L. Tang, Molybdenum disulfide (MoS₂) as a co-catalyst for photocatalytic degradation of organic contaminants: a review, *Process Saf. Environ. Protect.* 118 (2018) 40–58.
- [14] X. Meng, Z. Li, H. Zeng, J. Chen, Z. Zhang, MoS₂ quantum dots-interspersed Bi₂WO₆ heterostructures for visible light-induced detoxification and disinfection, *Appl. Catal. B: Environ.* 210 (2017) 160–172.
- [15] G. Zhang, H. Liu, J. Qu, J. Li, Two-dimensional layered MoS₂: rational design, properties and electrochemical applications, *Energy Environ. Sci.* 9 (2016) 1190–1209.

- [16] J. Theerthagiri, R.A. Senthil, B. Senthilkumar, A. Reddy Polu, J. Madhavan, M. Ashokkumar, Recent advances in MoS₂ nanostructured materials for energy and environmental applications – a review, *J. Solid State Chem.* 252 (2017) 43–71.
- [17] Z. Li, X. Meng, Z. Zhang, Recent development on MoS₂-based photocatalysis: a review, *J. Photochem. Photobiol. C: Photochem. Rev.* 35 (2018) 39–55.
- [18] Z. Liang, R. Shen, Y.H. Ng, P. Zhang, Q. Xiang, X. Li, A review on 2D MoS₂ cocatalysts in photocatalytic H₂ production, *J. Mater. Sci. Technol.* 56 (2020) 89–121.
- [19] R.J. Toh, Z. Sofer, J. Luxa, D. Sedmidubský, M. Pumera, 3R phase of MoS₂ and WS₂ outperforms the corresponding 2H phase for hydrogen evolution, *Chem. Commun.* 53 (2017) 3054–3057.
- [20] X. Li, H. Zhu, Two-dimensional MoS₂: properties, preparation, and applications, *J. Materomics* 1 (2015) 33–44.
- [21] S. Li, J. Sun, J. Guan, Strategies to improve electrocatalytic and photocatalytic performance of two-dimensional materials for hydrogen evolution reaction, *Chin. J. Catal.* 42 (2021) 511–556.
- [22] M. Chhowalla, H.S. Shin, G. Eda, L.-J. Li, K.P. Loh, H. Zhang, The chemistry of two-dimensional layered transition metal dichalcogenide nanosheets, *Nat. Chem.* 5 (2013) 263–275.
- [23] Y.J. Yuan, Z.K. Shen, S.T. Wu, Y.B. Su, L. Pei, Z.G. Ji, M.Y. Ding, W.F. Bai, Y.F. Chen, Z.T. Yu, Z.G. Zou, Liquid exfoliation of g-C₃N₄ nanosheets to construct 2D-2D MoS₂/g-C₃N₄ photocatalyst for enhanced photocatalytic H₂ production activity, *Appl. Catal. B: Environ.* 246 (2019) 120–128.
- [24] D. Voiry, M. Salehi, R. Silva, T. Fujita, M.W. Chen, T. Asefa, V.B. Shenoy, G. Eda, M. Chhowalla, Conducting MoS₂ nanosheets as catalysts for hydrogen evolution reaction, *Nano Lett.* 13 (2013) 6222–6227.
- [25] S. Yu, H.D. Xiong, K. Eshun, H. Yuan, Q.L. Li, Phase transition, effective mass and carrier mobility of MoS₂ monolayer under tensile strain, *Appl. Surf. Sci.* 325 (2015) 27–32.
- [26] M. Acerce, D. Voiry, M. Chhowalla, Metallic 1T phase MoS₂ nanosheets as supercapacitor electrode materials, *Nat. Nanotechnol.* 10 (2015) 313–318.
- [27] J.T. Zhu, J. Wu, Y.H. Sun, J.W. Huang, Y.F. Xia, H. Wang, H.B. Wang, Y. Wang, Q.H. Yia, G.F. Zou, Thickness-dependent bandgap tunable molybdenum disulfide films for optoelectronics, *RSC Adv.* 6 (2016) 110604–110609.
- [28] Y.Y. Li, S. Wu, J.W. Zheng, Y.K. Peng, D. Prabhakaran, R.A. Taylor, S.C.E. Tsang, 2D photocatalysts with tuneable supports for enhanced photocatalytic water splitting, *Mater. Today* 41 (2020) 34–43.
- [29] K.F. Mak, C. Lee, J. Hone, J. Shan, T.F. Heinz, Atomically thin MoS₂: a new direct-gap semiconductor, *Phys. Rev. Lett.* 105 (2010).
- [30] J.X. Huang, X.L. Pan, X.B. Liao, M.Y. Yan, B. Dunn, W. Luo, L.Q. Ma, In situ monitoring of the electrochemically induced phase transition of thermodynamically metastable 1T-MoS(2) at nanoscale, *Nanoscale* 12 (2020) 9246–9254.
- [31] J.C. Ma, Q.X. Zhang, J. Yang, S.Y. Feng, M. Lei, R.G. Quhe, Computational study of phase engineered transition metal dichalcogenides heterostructures, *Comput. Mater. Sci.* 142 (2018) 129–134.
- [32] F.A. Rasmussen, K.S. Thygesen, Computational 2D materials database: electronic structure of transition-metal dichalcogenides and oxides, *J. Phys. Chem. C* 119 (2015) 13169–13183.
- [33] R. Qian, H. Tong, J. Schneider, G. Zhou, T. Zhao, Y. Li, J. Yang, D.W. Bahnemann, J.H. Pan, Charge carrier trapping, recombination and transfer during TiO₂ photocatalysis: an overview, *Catal. Today* 335 (2019) 78–90.
- [34] C. Lee, H. Yan, L.E. Brus, T.F. Heinz, J. Hone, S. Ryu, Anomalous lattice vibrations of single-and few-layer MoS₂, *ACS Nano* 4 (2010) 2695–2700.
- [35] G. Eda, H. Yamaguchi, D. Voiry, T. Fujita, M. Chen, M. Chhowalla, Photoluminescence from chemically exfoliated MoS₂, *Nano Lett.* 11 (2011) 5111–5116.
- [36] K.S. Novoselov, A.K. Geim, S.V. Morozov, D. Jiang, Y. Zhang, S.V. Dubonos, I.V. Grigorieva, A.A. Firsov, Electric field effect in atomically thin carbon films, *Science* 306 (2004) 666.
- [37] G.Z. Magda, J. Pető, G. Dobrik, C. Hwang, L.P. Biró, L. Tapaszto, Exfoliation of large-area transition metal chalcogenide single layers, *Sci. Rep.* 5 (2015) 1–5.
- [38] L. Ottaviano, S. Palleschi, F. Perrozzi, G. D'Olimpio, F. Priante, M. Donarelli, P. Benassi, M. Nardone, M. Gonchigsuren, M. Gombosuren, A. Lucia, G. Moccia, O.A. Cacioppo, Mechanical exfoliation and layer number identification of MoS₂ revisited, *2D Mater.* 4 (2017), 045013.
- [39] H. Li, J. Wu, Z. Yin, H. Zhang, Preparation and applications of mechanically exfoliated single-layer and multilayer MoS₂ and WSe₂ nanosheets, *Acc. Chem. Res.* 47 (2014) 1067–1075.
- [40] X. Liu, T. Xu, X. Wu, Z. Zhang, J. Yu, H. Qiu, J.-H. Hong, C.-H. Jin, J.-X. Li, X.-R. Wang, Top-down fabrication of sub-nanometre semiconducting nanoribbons derived from molybdenum disulfide sheets, *Nat. Commun.* 4 (2013) 1–6.
- [41] Q. Zhang, L. Mei, X. Cao, Y. Tang, Z. Zeng, Intercalation and exfoliation chemistries of transition metal dichalcogenides, *J. Mater. Chem. A* 8 (2020) 15417–15444.
- [42] F.I. Alzakia, W. Jonhson, J. Ding, S.C. Tan, Ultrafast exfoliation of 2D materials by solvent activation and one-step fabrication of all-2D-material photodetectors by electrohydrodynamic printing, *ACS Appl. Mater. Interfaces* 12 (2020) 28840–28851.
- [43] X.J. Chua, M. Pumera, The effect of varying solvents for MoS₂ treatment on its catalytic efficiencies for HER and ORR, *Phys. Chem. Chem. Phys.* 19 (2017) 6610–6619.
- [44] S. Venkatram, C. Kim, A. Chandrasekaran, R. Ramprasad, Critical assessment of the Hildebrand and Hansen solubility parameters for polymers, *J. Chem. Inf. Model.* 59 (2019) 4188–4194.
- [45] E.D. Grayfer, M.N. Kozlova, V.E. Fedorov, Colloidal 2D nanosheets of MoS₂ and other transition metal dichalcogenides through liquid-phase exfoliation, *Adv. Colloid Interface Sci.* 245 (2017) 40–61.
- [46] Y. Li, X. Yin, W. Wu, Preparation of few-layer MoS₂ nanosheets via an efficient shearing exfoliation method, *Ind. Eng. Chem. Res.* 57 (2018) 2838–2846.
- [47] J. Sun, X. Li, W. Guo, M. Zhao, X. Fan, Y. Dong, C. Xu, J. Deng, Y. Fu, Synthesis methods of two-dimensional MoS₂: a brief review, *Crystals* 7 (2017).
- [48] A. Ambrosi, Z. Sofer, M. Pumera, Lithium intercalation compound dramatically influences the electrochemical properties of exfoliated MoS₂, *Small* 11 (2015) 605–612.
- [49] Y. Zhu, Y. Ji, Z. Ju, K. Yu, P.J. Ferreira, Y. Liu, G. Yu, Ultrafast intercalation enabled by strong solvent–host interactions: understanding solvent effect at the atomic level, *Angew. Chem. Int. Ed.* 58 (2019) 17205–17209.
- [50] E.Y. Martinez, K. Zhu, C.W. Li, Reversible electron doping of layered metal hydroxide nanoplates (M= Co, Ni) using n-butyllithium, *Nano Lett.* 20 (2020) 7580–7587.
- [51] J. Zou, F. Li, M.A. Bissett, F. Kim, L.J. Hardwick, Intercalation behaviour of Li and Na into 3-layer and multilayer MoS₂ flakes, *Electrochim. Acta* 331 (2020) 135284.
- [52] C. Wang, H. Lu, K. Tang, Z. Mao, Q. Li, X. Wang, C. Yan, Atom removal on the basal plane of layered MoS₂ leading to extraordinarily enhanced electrocatalytic performance, *Electrochim. Acta* 336 (2020) 135740.
- [53] A. Abraham, L. Wang, C.D. Quilty, D.M. Lutz, A.H. McCarthy, C.R. Tang, M.R. Dunkin, L.M. Housell, E.S. Takeuchi, A.C. Marschilok, K.J. Takeuchi, Defect control in the synthesis of 2D MoS₂ nanosheets: polysulfide trapping in composite sulfur cathodes for Li–S batteries, *ChemSusChem* 13 (2020) 1517–1528.
- [54] T.-s. Song, L. Fu, N. Wan, J. Wu, J. Xie, Hydrothermal synthesis of MoS₂ nanoflowers for an efficient microbial electrosynthesis of acetate from CO₂, *J. CO₂ Util.* 41 (2020) 101231.
- [55] Q. Huang, Y. Fang, J. Shi, Y. Liang, Y. Zhu, G. Xu, Flower-like molybdenum disulfide for polarity-triggered accumulation/release of small molecules, *ACS Appl. Mater. Interfaces* 9 (2017) 36431–36437.
- [56] Y.H. Lee, X.Q. Zhang, W. Zhang, M.T. Chang, C.T. Lin, K.D. Chang, Y.C. Yu, J.T.W. Wang, C.S. Chang, L.J. Li, Synthesis of large-area MoS₂ atomic layers with chemical vapor deposition, *Adv. Mater.* 24 (2012) 2320–2325.
- [57] C. Xie, P. Yang, Y. Huan, F. Cui, Y. Zhang, Roles of salts in the chemical vapor deposition synthesis of two-dimensional transition metal chalcogenides, *Dalton Trans.* 49 (2020) 10319–10327.
- [58] L. Lei, D. Huang, G. Zeng, M. Cheng, D. Jiang, C. Zhou, S. Chen, W. Wang, A fantastic two-dimensional MoS₂ material based on the inert basal planes activation: electronic structure, synthesis strategies, catalytic active sites, catalytic and electronics properties, *Coord. Chem. Rev.* 399 (2019) 213020.
- [59] M.A. Lukowski, A.S. Daniel, F. Meng, A. Forticaux, L. Li, S. Jin, Enhanced hydrogen evolution Catalysis from chemically exfoliated metallic MoS₂ nanosheets, *J. Am. Chem. Soc.* 135 (2013) 10274–10277.
- [60] C.A. Beaudette, J.T. Held, K.A. Mkoyan, U.R. Kortshagen, Nonthermal plasma-enhanced chemical vapor deposition of two-dimensional molybdenum disulfide, *ACS Omega* 5 (2020) 21853–21861.
- [61] Y. Yang, H. Pu, T. Lin, L. Li, S. Zhang, G. Sun, Growth of monolayer MoS₂ films in a quasi-closed crucible encapsulated substrates by chemical vapor deposition, *Chem. Phys. Lett.* 679 (2017) 181–184.
- [62] J. Sitek, J. Płocharski, I. Pasternak, A.P. Gertych, C. McAleese, B.R. Conran, M. Zdrojek, W. Strupinski, Substrate-induced variances in morphological and structural properties of MoS₂Grown by chemical vapor deposition on epitaxial graphene and SiO₂, *ACS Appl. Mater. Interfaces* 12 (2020) 45101–45110.
- [63] L. Liu, J. Wu, L. Wu, M. Ye, X. Liu, Q. Wang, S. Hou, P. Lu, L. Sun, J. Zheng, L. Xing, L. Gu, X. Jiang, L. Xie, L. Jiao, Phase-selective synthesis of 1T' MoS₂ monolayers and heterophase bilayers, *Nat. Mater.* 17 (2018) 1108–1114.
- [64] L. Zheng, F. Teng, X. Ye, H. Zheng, X. Fang, Photo/electrochemical applications of metal sulfide/TiO₂ heterostructures, *Adv. Energy Mater.* 10 (2020) 1902355.
- [65] V. Kumaravel, J. Bartlett, S.C. Pillai, Photoelectrochemical conversion of carbon dioxide (CO₂) into fuels and value-added products, *ACS Energy Lett.* 5 (2020) 486–519.
- [66] K.M. Nair, V. Kumaravel, S.C. Pillai, Carbonaceous cathode materials for electro-Fenton technology: mechanism, kinetics, recent advances, opportunities and challenges, *Chemosphere* 269 (2021) 129325.
- [67] Z. Yang, T. Qin, Y. Niu, Y. Zhang, C. Zhang, P. Li, M. Zhu, Y. Jia, Q. Li, Flexible visible-light-driven photoelectrochemical biosensor based on molecularly imprinted nanoparticle intercalation-modulated graphene fiber for ultra-sensitive urea detection, *Carbon* 157 (2020) 457–465.
- [68] S. Kunwar, S. Pandit, J.H. Jeong, J. Lee, Hybrid CoP₂–Pt–FTO nanoarchitecture for bifunctional electrocatalysts in H₂ generation by water splitting, *Mater. Today Sustain.* 9 (2020) 100045.
- [69] J. Joy, J. Mathew, S.C. George, Nanomaterials for photoelectrochemical water splitting – review, *Int. J. Hydrogen Energy* 43 (2018) 4804–4817.
- [70] T. Hisatomi, J. Kubota, K. Domen, Recent advances in semiconductors for photocatalytic and photoelectrochemical water splitting, *Chem. Soc. Rev.* 43 (2014) 7520–7535.

- [71] S. Ye, C. Ding, R. Chen, F. Fan, P. Fu, H. Yin, X. Wang, Z. Wang, P. Du, C. Li, Mimicking the key functions of photosystem II in artificial photosynthesis for photoelectrocatalytic water splitting, *J. Am. Chem. Soc.* 140 (2018) 3250–3256.
- [72] S. Shen, J. Chen, M. Wang, X. Sheng, X. Chen, X. Feng, S.S. Mao, Titanium dioxide nanostructures for photoelectrochemical applications, *Prog. Mater. Sci.* 98 (2018) 299–385.
- [73] X. Li, J. Yu, J. Low, Y. Fang, J. Xiao, X. Chen, Engineering heterogeneous semiconductors for solar water splitting, *J. Mater. Chem. A* 3 (2015) 2485–2534.
- [74] Y. Qu, X. Song, X. Chen, X. Fan, G. Zhang, Tuning charge transfer process of MoS₂ photoanode for enhanced photoelectrochemical conversion of ammonia in water into gaseous nitrogen, *Chem. Eng. J.* 382 (2020) 123048.
- [75] F. Gong, S. Ye, M. Liu, J. Zhang, L. Gong, G. Zeng, E. Meng, P. Su, K. Xie, Y. Zhang, J. Liu, Boosting electrochemical oxygen evolution over yolk-shell structured O–MoS₂ nanoreactors with sulfur vacancy and decorated Pt nanoparticles, *Nano Energy* 78 (2020) 105284.
- [76] L.A. King, W. Zhao, M. Chhowalla, D.J. Riley, G. Eda, Photoelectrochemical properties of chemically exfoliated MoS₂, *J. Mater. Chem. A* 1 (2013) 8935–8941.
- [77] M. Jalali, R.S. Moakhar, T. Abdelfattah, E. Filine, S.S. Mahshid, S. Mahshid, Nanopattern-assisted direct growth of peony-like 3D MoS₂/Au composite for nonenzymatic photoelectrochemical sensing, *ACS Appl. Mater. Interfaces* 12 (2020) 7411–7422.
- [78] S.S.M. Bhat, S.A. Pawar, D. Potphode, C.-K. Moon, J.M. Suh, C. Kim, S. Choi, D.S. Patil, J.-J. Kim, J.C. Shin, H.W. Jang, Substantially enhanced photoelectrochemical performance of TiO₂ nanorods/CdS nanocrystals heterojunction photoanode decorated with MoS₂ nanosheets, *Appl. Catal. B: Environ.* 259 (2019) 118102.
- [79] A. Kagkoura, J. Hernandez-Ferrer, A.M. Benito, W.K. Maser, N. Tagmatarchis, In-situ growth and immobilization of CdS nanoparticles onto functionalized MoS₂: preparation, characterization and fabrication of photoelectrochemical cells, *Chem. Asian J.* 15 (2020) 2350–2356.
- [80] X. Hu, X. Zeng, Y. Liu, J. Lu, S. Yuan, Y. Yin, J. Hu, D.T. McCarthy, X. Zhang, Nano-layer based 1T-rich MoS₂/g-C₃N₄ co-catalyst system for enhanced photocatalytic and photoelectrochemical activity, *Appl. Catal. B: Environ.* 268 (2020) 118466.
- [81] P.C. Sherrill, P. Palczynski, M.S. Sokolikova, F. Reale, F.M. Pesci, M. Och, C. Mattevi, Large-area CVD MoS₂/WS₂ heterojunctions as a photoelectrocatalyst for salt-water oxidation, *ACS Appl. Energy Mater.* 2 (2019) 5877–5882.
- [82] G. Paulraj, P.S. Venkatesh, P. Dharmaraj, S. Gopalakrishnan, K. Jeganathan, Stable and highly efficient MoS₂/Si NWs hybrid heterostructure for photoelectrocatalytic hydrogen evolution reaction, *Int. J. Hydrogen Energy* 45 (2020) 1793–1801.
- [83] U. Gupta, C.N.R. Rao, Hydrogen generation by water splitting using MoS₂ and other transition metal dichalcogenides, *Nano Energy* 41 (2017) 49–65.
- [84] K.C. Christoforidis, P. Fornasiero, Photocatalytic hydrogen production: a rift into the future energy supply, *ChemCatChem* 9 (2017) 1523–1544.
- [85] C. Huang, W. Yao, T. Ali, N. Muradov, Development of efficient photoreactors for solar hydrogen production, *Sol. Energy* 85 (2011) 19–27.
- [86] Y. Goto, T. Hisatomi, Q. Wang, T. Higashi, K. Ishikiriyama, T. Maeda, Y. Sakata, S. Okunaka, H. Tokudome, M. Katayama, A particulate photocatalyst water-splitting panel for large-scale solar hydrogen generation, *Joule* 2 (2018) 509–520.
- [87] Y. Li, S.C.E. Tsang, Recent progress and strategies for enhancing photocatalytic water splitting, *Mater. Today Sustain.* 9 (2020).
- [88] D. Jing, L. Guo, L. Zhao, X. Zhang, H. Liu, M. Li, S. Shen, G. Liu, X. Hu, X. Zhang, Efficient solar hydrogen production by photocatalytic water splitting: from fundamental study to pilot demonstration, *Int. J. Hydrogen Energy* 35 (2010) 7087–7097.
- [89] S. Sorcar, Y. Hwang, J. Lee, H. Kim, K.M. Grimes, C.A. Grimes, J.W. Jung, C.H. Cho, T. Majima, M.R. Hoffmann, S.I. In, CO₂, water, and sunlight to hydrocarbon fuels: a sustained sunlight to fuel (Joule-to-Joule) photoconversion efficiency of 1%, *Energy Environ. Sci.* 12 (2019) 2685–2696.
- [90] S. Choi, K.C. Kwon, S.Y. Kim, H.W. Jang, Tailoring catalytic activities of transition metal disulfides for water splitting, *FlatChem* 4 (2017) 68–80.
- [91] M.Z. Selcuk, M.S. Boroglu, I. Boz, Hydrogen production by photocatalytic water-splitting using nitrogen and metal co-doped TiO₂ powder photocatalyst, *React. Kinet. Mech. Catal.* 106 (2012) 313–324.
- [92] P. Cheng, Z. Yang, H. Wang, W. Cheng, M. Chen, W. Shangguan, G. Ding, TiO₂-graphene nanocomposites for photocatalytic hydrogen production from splitting water, *Int. J. Hydrogen Energy* 37 (2012) 2224–2230.
- [93] S. Ye, C. Ding, M. Liu, A. Wang, Q. Huang, C. Li, Water oxidation catalysts for artificial photosynthesis, *Adv. Mater.* 31 (2019) 1–33.
- [94] S. Ye, C. Ding, C. Li, Chapter One – artificial photosynthesis systems for catalytic water oxidation, in: R. van Eldik, C.D. Hubbard (Eds.), *Advances in Inorganic Chemistry*, Academic Press, 2019, pp. 3–59.
- [95] Z. Zhu, C.-T. Kao, B.-H. Tang, W.-C. Chang, R.-J. Wu, Efficient hydrogen production by photocatalytic water-splitting using Pt-doped TiO₂ hollow spheres under visible light, *Ceram. Int.* 42 (2016) 6749–6754.
- [96] Y. Shinde, S. Wadhai, A. Ponkshe, S. Kapoor, P. Thakur, Decoration of Pt on the metal free RGO-TiO₂ composite photocatalyst for the enhanced photocatalytic hydrogen evolution and photocatalytic degradation of pharmaceutical pollutant beta blocker, *Int. J. Hydrogen Energy* 43 (2018) 4015–4027.
- [97] B. Liu, S. Su, W. Zhou, Y. Wang, D. Wei, L. Yao, Y. Ni, M. Cao, C. Hu, Photo-reduction assisted synthesis of W-doped TiO₂ coupled with Au nanoparticles for highly efficient photocatalytic hydrogen evolution, *CrystEngComm* 19 (2017) 675–683.
- [98] R.W. Liang, S.G. Luo, F.F. Jing, L.J. Shen, N. Qin, L. Wu, A simple strategy for fabrication of Pd@MIL-100(Fe) nanocomposite as a visible-light-driven photocatalyst for the treatment of pharmaceuticals and personal care products (PPCPs), *Appl. Catal. B: Environ.* 176 (2015) 240–248.
- [99] T. Sun, E. Liu, X. Liang, X. Hu, J. Fan, Enhanced hydrogen evolution from water splitting using Fe-Ni codoped and Ag deposited anatase TiO₂ synthesized by solvothermal method, *Appl. Surf. Sci.* 347 (2015) 696–705.
- [100] Y.P. Liu, Y.H. Li, F. Peng, Y. Lin, S.Y. Yang, S.S. Zhang, H.J. Wang, Y.H. Cao, H. Yu, 2H-and 1T-mixed phase few-layer MoS₂ as a superior to Pt co-catalyst coated on TiO₂ nanorod arrays for photocatalytic hydrogen evolution, *Appl. Catal. B: Environ.* 241 (2019) 236–245.
- [101] A. Elizabeth, H. Conradi, S.K. Sahoo, T. Kodalle, C.A. Kaufmann, T.D. Kühne, H. Mirhosseini, D. Abou-Ras, H. Möning, Correlating facet orientation, defect-level density and dipole layer formation at the surface of polycrystalline CuInSe₂ thin films, *Acta Mater.* 200 (2020) 463–470.
- [102] J. Li, G. Zhan, Y. Yu, L. Zhang, Superior visible light hydrogen evolution of Janus bilayer junctions via atomic-level charge flow steering, *Nat. Commun.* 7 (2016) 1–9.
- [103] L. Su, L. Luo, J. Wang, T. Song, W. Tu, Z.-j. Wang, Lamellar flower-like porous MoS₂ as an efficient cocatalyst to boost photocatalytic hydrogen evolution of CdS, *Catal. Sci. Technol.* (2021) 1292–1297.
- [104] W.J. Zhou, Z.Y. Yin, Y.P. Du, X. Huang, Z.Y. Zeng, Z.X. Fan, H. Liu, J.Y. Wang, H. Zhang, Synthesis of few-layer MoS₂ nanosheet-coated TiO₂ nanobelt heterostructures for enhanced photocatalytic activities, *Small* 9 (2013) 140–147.
- [105] J. Zhang, Z. Zhu, X. Feng, Construction of two-dimensional MoS₂/CdS p-n nanohybrids for highly efficient photocatalytic hydrogen evolution, *Chem. – Eur. J.* 20 (2014) 10632–10635.
- [106] R.K. Chava, J.Y. Do, M. Kang, Smart hybridization of Au coupled CdS nanorods with few layered MoS₂ nanosheets for high performance photocatalytic hydrogen evolution reaction, *ACS Sustain. Chem. Eng.* 6 (2018) 6445–6457.
- [107] C. Zhu, Y. Wang, Z. Jiang, F. Xu, Q. Xian, C. Sun, Q. Tong, W. Zou, X. Duan, S. Wang, CeO₂ nanocrystal-modified layered MoS₂/g-C₃N₄ as OD/2D ternary composite for visible-light photocatalytic hydrogen evolution: interfacial consecutive multi-step electron transfer and enhanced H₂O reactant adsorption, *Appl. Catal. B: Environ.* 259 (2019) 118072.
- [108] H. Li, G. Wang, H. Gong, Z. Jin, Phosphated 2D MoS₂ nanosheets and 3D NiTiO₃ nanorods for efficient photocatalytic hydrogen evolution, *ChemCatChem* 12 (2020) 5492–5503.
- [109] Z. Liang, Y. Xue, Y. Guo, G. Zhang, H. Cui, J. Tian, Rationalizing and controlling the phase transformation of semi-metallic 1T'-phase and semi-conductive 2H-phase MoS₂ as cocatalysts for photocatalytic hydrogen evolution, *Chem. Eng. J.* 396 (2020) 125344.
- [110] Z. Wei, M. Xu, J. Liu, W. Guo, Z. Jiang, W. Shangguan, Simultaneous visible-light-induced hydrogen production enhancement and antibiotic wastewater degradation using MoS₂@Zn_xCd_{1-x}S: solid-solution-assisted photocatalysis, *Chin. J. Catal.* 41 (2020) 103–113.
- [111] X. Xin, Y. Song, S. Guo, Y. Zhang, B. Wang, Y. Wang, X. Li, One-step synthesis of P-doped MoS₂ for efficient photocatalytic hydrogen production, *J. Alloys Compd.* 829 (2020) 154635.
- [112] Y. Chen, F. Su, H. Xie, R. Wang, C. Ding, J. Huang, Y. Xu, L. Ye, One-step construction of S-scheme heterojunctions of N-doped MoS₂ and S-doped g-C₃N₄ for enhanced photocatalytic hydrogen evolution, *Chem. Eng. J.* 404 (2021) 126498.
- [113] G. Guan, E. Ye, M. You, Z. Li, Hybridized 2D nanomaterials toward highly efficient photocatalysis for degrading pollutants: current status and future perspectives, *Small* 16 (2020) 1907087.
- [114] Q. Li, N. Zhang, Y. Yang, G. Wang, D.H.L. Ng, High efficiency photocatalysis for pollutant degradation with MoS₂/C₃N₄ heterostructures, *Langmuir* 30 (2014) 8965–8972.
- [115] X. Zhang, S.Y. Teng, A.C. Loy, B.S. How, W.D. Leong, X. Tao, Transition metal dichalcogenides for the application of pollution reduction: a review, *Nanomaterials* 10 (2020).
- [116] Y. Lin, P. Ren, C. Wei, Fabrication of MoS₂/TiO₂ heterostructures with enhanced photocatalytic activity, *CrystEngComm* 21 (2019) 3439–3450.
- [117] G. Guan, M. You, X. Liu, Y.-L. Wu, E. Ye, Z. Li, Tris-stabilized MoS₂ nanosheets with robust dispersibility and facile surface functionalization, *Adv. Mater. Interfaces* 6 (2019) 1900585.
- [118] Z. Xia, Y. Tao, Z. Pan, X. Shen, Enhanced photocatalytic performance and stability of 1T MoS₂ transformed from 2H MoS₂ via Li intercalation, *Results Phys.* 12 (2019) 2218–2224.
- [119] S. Saha, N. Chaudhary, H. Mittal, G. Gupta, M. Khanuja, Inorganic–organic nanohybrid of MoS₂-PANI for advanced photocatalytic application, *Int. Nano Lett.* 9 (2019) 127–139.
- [120] M.D.J. Quinn, N.H. Ho, S.M. Notley, Aqueous dispersions of exfoliated molybdenum disulfide for use in visible-light photocatalysis, *ACS Appl. Mater. Interfaces* 5 (2013) 12751–12756.
- [121] G. Li, P. Lei, M. Zhou, W. Wang, D. Li, C. Yang, N. Hua, S. Chen, Effect of molecular weight of polyethylene glycol on the sheet-thickness and

- photocatalytic performance of MoS₂ nanoparticles, *Appl. Surf. Sci.* 469 (2019) 312–315.
- [122] W. Zhang, X. Xiao, Y. Li, X. Zeng, L. Zheng, C. Wan, Liquid-exfoliation of layered MoS₂ for enhancing photocatalytic activity of TiO₂/g-C₃N₄ photocatalyst and DFT study, *Appl. Surf. Sci.* 389 (2016) 496–506.
- [123] X. Hu, H. Zhao, J. Tian, J. Gao, Y. Li, H. Cui, Synthesis of few-layer MoS₂ nanosheets-coated TiO₂ nanosheets on graphite fibers for enhanced photocatalytic properties, *Sol. Energy Mater. Sol. Cell.* 172 (2017) 108–116.
- [124] X. Liu, Z. Xing, H. Zhang, W. Wang, Y. Zhang, Z. Li, X. Wu, X. Yu, W. Zhou, Fabrication of 3D mesoporous black TiO₂/MoS₂/TiO₂ nanosheets for visible-light-driven photocatalysis, *ChemSusChem* 9 (2016) 1118–1124.
- [125] J. Dong, J. Huang, A. Wang, G.V. Biesold-McGee, X. Zhang, S. Gao, S. Wang, Y. Lai, Z. Lin, Vertically-aligned Pt-decorated MoS₂ nanosheets coated on TiO₂ nanotube arrays enable high-efficiency solar-light energy utilization for photocatalysis and self-cleaning SERS devices, *Nano Energy* 71 (2020) 104579, 104579.
- [126] Z. Wang, B. Mi, Environmental applications of 2D molybdenum disulfide (MoS₂) nanosheets, *Environ. Sci. Technol.* 51 (2017) 8229–8244.
- [127] M.A. Islam, J. Church, C. Han, H.-S. Chung, E. Ji, J.H. Kim, N. Choudhary, G.-H. Lee, W.H. Lee, Y. Jung, Noble metal-coated MoS₂ nanofilms with vertically-aligned 2D layers for visible light-driven photocatalytic degradation of emerging water contaminants, *Sci. Rep.* 7 (2017) 1–10.
- [128] M. Chhowalla, G.A.J. Amaratunga, Thin films of fullerene-like MoS₂ nanoparticles with ultra-low friction and wear, *Nature* 407 (2000) 164–167.
- [129] S. Banerjee, D.D. Dionysiou, S.C. Pillai, Self-cleaning applications of TiO₂ by photo-induced hydrophilicity and photocatalysis, *Appl. Catal. B: Environ.* 176–177 (2015) 396–428.
- [130] R.N. Wenzel, Resistance of solid surfaces to wetting by water, *Ind. Eng. Chem.* 28 (1936) 988–994.
- [131] A.B.D. Cassie, S. Baxter, Wettability of porous surfaces, *Trans. Faraday Soc.* 40 (1944) 546–551.
- [132] I. Alam, L.M. Guiney, M.C. Hersam, I. Chowdhury, Antifouling properties of two-dimensional molybdenum disulfide and graphene oxide, *Environ. Sci.: Nano* 5 (2018) 1628–1639.
- [133] Y. Chao, W. Zhu, X. Wu, F. Hou, S. Xun, P. Wu, H. Ji, H. Xu, H. Li, Application of graphene-like layered molybdenum disulfide and its excellent adsorption behavior for doxycycline antibiotic, *Chem. Eng. J.* 243 (2014) 60–67.
- [134] Y. Ding, Y. Zhou, W. Nie, P. Chen, MoS₂-GO nanocomposites synthesized via a hydrothermal hydrogel method for solar light photocatalytic degradation of methylene blue, *Appl. Surf. Sci.* 357 (2015) 1606–1612.
- [135] Y. Zhao, X. Zhang, C. Wang, Y. Zhao, H. Zhou, J. Li, H. Jin, The synthesis of hierarchical nanostructured MoS₂/Graphene composites with enhanced visible-light photo-degradation property, *Appl. Surf. Sci.* 412 (2017) 207–213.
- [136] Z. Cai, A.D. Dwivedi, W.-N. Lee, X. Zhao, W. Liu, M. Sillanpää, D. Zhao, C.-H. Huang, J. Fu, Application of nanotechnologies for removing pharmaceutically active compounds from water: development and future trends, *Environ. Sci.: Nano* 5 (2018) 27–47.
- [137] Z.-G. Zhang, H. Liu, X.-X. Wang, J. Zhang, M. Yu, S. Ramakrishna, Y.-Z. Long, One-step low temperature hydrothermal synthesis of flexible TiO₂/PVDF@MoS₂ core-shell heterostructured fibers for visible-light-driven photocatalysis and self-cleaning, *Nanomaterials* 9 (2019) 431.
- [138] M. Yu, P. Xu, J. Yang, L. Ji, C. Li, Self-growth of MoS₂ sponge for highly efficient photothermal cleanup of high-viscosity crude oil spills, *Adv. Mater. Interfaces* 7 (2020) 1901671.
- [139] T.M. Chou, S.W. Chan, Y.J. Lin, P.K. Yang, C.C. Liu, J.M. Wu, J.T. Lee, Z.H. Lin, A highly efficient Au-MoS₂ nanocatalyst for tunable piezocatalytic and photocatalytic water disinfection, *Nano Energy* 57 (2019) 14–21.
- [140] F. Alimohammadi, G.M. Sharifian, N.H. Attanayake, A.C. Thenuwara, Y. Gogotsi, B. Anasori, D.R. Strongin, Antimicrobial properties of 2D MnO₂ and MoS₂ nanomaterials vertically aligned on graphene materials and Ti3C₂ MXene, *Langmuir* 34 (2018) 7192–7200.
- [141] C. Liu, D. Kong, P.-C. Hsu, H. Yuan, H.-W. Lee, Y. Liu, H. Wang, S. Wang, K. Yan, D. Lin, P.A. Maraccini, K.M. Parker, A.B. Boehm, Y. Cui, Rapid water disinfection using vertically aligned MoS₂ nanofilms and visible light, *Nat. Nanotechnol.* 11 (2016) 1098–1104.
- [142] M.J. Hajipour, K.M. Fromm, A. Akbar Ashkarran, D. Jimenez de Aberasturi, I.R.d. Laramendi, T. Rojo, V. Serpooshan, W.J. Parak, M. Mahmoudi, Antibacterial properties of nanoparticles, *Trends Biotechnol.* 30 (2012) 499–511.
- [143] J. Jeong, J.Y. Kim, J. Yoon, The role of reactive oxygen species in the electrochemical inactivation of microorganisms, *Environ. Sci. Technol.* 40 (2006) 6117–6122.
- [144] R. Canaparo, F. Foglietta, T. Limongi, L. Serpe, Biomedical applications of reactive oxygen species generation by metal nanoparticles, *Materials* 14 (2021) 53.
- [145] V. Krishna, S. Pumprueg, S.H. Lee, J. Zhao, W. Sigmund, B. Koopman, B.M. Moudgil, Photocatalytic disinfection with titanium dioxide coated multi-wall carbon nanotubes, *Process Saf. Environ. Protect.* 83 (2005) 393–397.
- [146] H. Yan, L. Liu, R. Wang, W. Zhu, X. Ren, L. Luo, X. Zhang, S. Luo, X. Ai, J. Wang, Binary composite MoS₂/TiO₂ nanotube arrays as a recyclable and efficient photocatalyst for solar water disinfection, *Chem. Eng. J.* 401 (2020) 126052.
- [147] X. Yang, J. Li, T. Liang, C. Ma, Y. Zhang, H. Chen, N. Hanagata, H. Su, M. Xu, Antibacterial activity of two-dimensional MoS₂ sheets, *Nanoscale* 6 (2014) 10126–10133.
- [148] S. Pandit, S. Karunakaran, S.K. Boda, B. Basu, M. De, High antibacterial activity of functionalized chemically exfoliated MoS₂, *ACS Appl. Mater. Interfaces* 8 (2016) 31567.
- [149] Y. Zhang, P. Ju, L. Hao, X. Zhai, F. Jiang, C. Sun, Novel Z-scheme MoS₂/Bi2WO6 heterojunction with highly enhanced photocatalytic activity under visible light irradiation, *J. Alloys Compd.* 854 (2021) 157224.
- [150] M. Tong, F. Liu, Q. Dong, Z. Ma, W. Liu, Magnetic Fe₃O₄-deposited flower-like MoS₂ nanocomposites for the Fenton-like *Escherichia coli* disinfection and diclofenac degradation, *J. Hazard Mater.* 385 (2020) 121604.
- [151] M.B. Askari, A.F. Kalourazi, M. Seifi, S.S. Shahangian, N. Askari, T.J. Manjili, Hydrothermal Synthesis of molybdenum disulfide (MoS₂) and study of structure, optical, electrical and high Antibacterial properties, *Optik* 174 (2018) 154–162.
- [152] S. Fu, W. Yuan, Y. Yan, H. Liu, X. Shi, F. Zhao, J. Zhou, Highly efficient visible-light photoactivity of Z-scheme MoS₂/Ag₂CO₃ photocatalysts for organic pollutants degradation and bacterial inactivation, *J. Environ. Manag.* 252 (2019) 109654.
- [153] P. Cheng, Q. Zhou, X. Hu, S. Su, X. Wang, M. Jin, L. Shui, X. Gao, Y. Guan, R. Nözel, G. Zhou, Z. Zhang, J. Liu, Transparent glass with the growth of pyramid-type MoS₂ for highly efficient water disinfection under visible-light irradiation, *ACS Appl. Mater. Interfaces* 10 (2018) 23444–23450.
- [154] S.R. Ali, S. Pandit, M. De, 2D-MoS₂-Based β -lactamase inhibitor for combination therapy against drug-resistant bacteria, *ACS Appl. Bio Mater.* 1 (2018) 967–974.
- [155] S.K. Ray, D. Dhakal, J. Hur, S.W. Lee, Visible light driven MoS₂/ α -NiMoO₄ ultra-thin nanoneedle composite for efficient *Staphylococcus aureus* inactivation, *J. Hazard Mater.* 385 (2020) 121553.
- [156] J. Li, J. Zheng, Y. Yu, Z. Su, L. Zhang, X. Chen, Facile synthesis of rGO-MoS(2)-Ag nanocomposites with long-term antimicrobial activities, *Nanotechnology* 31 (2020) 125101.
- [157] H. Wang, H. Qi, M. Zhu, S. Gong, Z. Huang, Y. Zhang, X. Chen, X.a. Jiao, MoS₂ decorated nanocomposite: Fe₂O₃@MoS₂ inhibits the conjugative transfer of antibiotic resistance genes, *Ectocotoxol. Environ. Saf.* 186 (2019) 109781.
- [158] H. Wang, H. Qi, S. Gong, Z. Huang, C. Meng, Y. Zhang, X. Chen, X.a. Jiao, Fe₂O₄ composited with MoS₂ blocks horizontal gene transfer, *Colloids Surf. B: Biointerfaces* 185 (2020) 110569.
- [159] X. Wang, M. Hong, F. Zhang, Z. Zhuang, Y. Yu, Recyclable nanoscale zero valent iron doped g-C₃N₄/MoS₂ for efficient photocatalysis of RhB and Cr(VI) driven by visible light, *ACS Sustain. Chem. Eng.* 4 (2016) 4055–4063.
- [160] K.K. Paul, N. Sreekanth, R.K. Biroju, T.N. Narayanan, P.K. Giri, Solar light driven photoelectrocatalytic hydrogen evolution and dye degradation by metal-free few-layer MoS₂ nanoflower/TiO₂(B) nanobelts heterostructure, *Sol. Energy Mater. Sol. Cell.* 185 (2018) 364–374.
- [161] D. Mu, Z. Chen, H. Shi, N. Tan, Construction of flower-like MoS₂/Fe₃O₄/rGO composite with enhanced photo-Fenton like catalyst performance, *RSC Adv.* 8 (2018) 36625–36631.
- [162] F. Xu, B. Zhu, B. Cheng, J. Yu, J. Xu, 1D/2D TiO₂/MoS₂ hybrid nanostructures for enhanced photocatalytic CO₂ reduction, *Adv. Opt. Mater.* 6 (2018) 8–15.
- [163] H. Jung, K.M. Cho, K.H. Kim, H.W. Yoo, A. Al-Saggaf, I. Gereige, H.T. Jung, Highly efficient and stable CO₂ reduction photocatalyst with a hierarchical structure of mesoporous TiO₂ on 3D graphene with few-layered MoS₂, *ACS Sustain. Chem. Eng.* 6 (2018) 5718–5724.



Nishanth Thomas is a Ph.D. candidate in the Nanotechnology and Bio-Engineering Research Group at the Institute of Technology Sligo, Ireland. He completed his BSMS dual degree in Chemistry (major) with Biology minor from Indian Institute of Science Education and Research (IISER) Bhopal. During his master's thesis, he investigated the shape-selective synthesis of silver nanostructures by a modified polyol method. Currently, he is working in the EU-Horizon 2020 PANI Water Project for developing Advanced Oxidation Processes (AOPs) for the removal of antimicrobial-resistant organisms from water. His research interest involves the design of unique nanomaterials for the sustainable environment and energy applications.



Snehamol Mathew received her bachelor's degree in chemistry and master's degree in Nanoscience and Nanotechnology from Mahatma Gandhi University, India. For her master's project, she worked on developing a polyglycerol-based macromolecular iron chelator at the University of British Columbia, Canada. She is currently working as a Renewable engine PhD candidate funded by the EU INTERREG VA Programme on investigating the fabrication of modified TiO₂ nanomaterials for photocatalytic hydrogen production and antimicrobial coatings. Her research focuses on the synthesis, modification, and characterization of nanomaterials for energy and environmental applications.



Keerthi M. Nair graduated with a dual degree of Bachelor of Science and Master of science in Chemistry from Indian Institute of Science Education and Research, Thiruvananthapuram (IISER Tvm). Currently, she is a Graduate student under EU-funded EU-Horizon 2020 PANI Water project, under the supervision of Prof. Suresh C. Pillai, at the Institute of Technology, Sligo. Her Ph. D work is on the development of novel electrode materials for electro Fenton reactions and electrochemical oxidation mechanisms in wastewater, along with the development of novel routes for the photo- and electro-generation of oxidizing species.



Kris O'Dowd joined I.T. Sligo as a postgraduate working on the optimization of the photo-Fenton process for the removal of antimicrobial-resistant organisms from water. This research is part of the Horizon 2020 PANI-Water project that is focused on the photo-irradiation and novel-based innovations for water treatment. The project aims to develop and validate prototypes for the removal of contaminants from wastewater and drinking water in peri-urban and rural areas in India. The photo-Fenton process is an advanced oxidation process that uses hydrogen peroxide, iron, and light to create a hydroxyl radical. This nonselective radical has been used extensively in the breakdown of organic chemicals and is now being investigated for its use in the elimination of microorganisms. The research will focus on optimizing a process that is traditionally used at an acidic pH, at a neutral pH to allow ease of use in rural communities.



Parnia Forouzandeh is a PhD candidate in the Department of Environmental Science at the Institute of Technology Sligo (IT Sligo), in the Nanotechnology and Bio-engineering Research Division, recipient of the 2019 president bursary fellowship. Her research entitled "2D Nanomaterials for efficient asymmetric supercapacitors.", which focuses on synthesis, modification, and characterization of novel two-dimensional materials and utilizing these nanostructures for energy applications beyond supercapacitor devices. Parnia obtained a B.Sc. in the "chemical engineering-inorganic chemical industry" and the M.Sc. degree in "chemical nano-engineering" (2019), under the European Erasmus Mundus Joint program in universities of Aix-Marseille University

(France), the Wroclaw University of Science and Technology (Poland), and the University of Rome Tor Vergata (Italy).



Amit Goswami is a doctoral candidate in the 'Department of Mechanical and Manufacturing Engineering' at the Institute of technology, Sligo, Ireland. He completed his graduation and post-graduation from Indian Institute of Information Technology, Design and Manufacturing, Kancheepuram, India, in 'Mechanical Engineering' as his major. During his specialization in 'Advanced Manufacturing' in his Master's, he investigated the heat transfer aspects of a freeze casting porous ceramic manufacturing method. Currently, he is working on a project titled 'Use of surface coatings in phase-change enhancement'. His area of interest lies in the modification of surfaces for enhanced heat transfer, antifouling, and self-cleaning behavior.



Gerard McGranaghan is a Lecturer in Mechanical and Manufacturing Engineering at IT Sligo, Ireland. He received his PhD from Trinity College Dublin in 2013. His areas of interest include convective flow boiling, two-phase heat transfer, enhanced surfaces, additive manufacturing, and energy.



Suresh C. Pillai obtained his Ph.D. from Trinity College Dublin and completed his postdoctoral research at California Institute of Technology (Caltech, USA). Upon completion of this appointment, he returned to Trinity College Dublin as a Research Fellow before joining CREST-TU Dublin as a Senior Scientist in April 2004. He has joined at IT Sligo in 2013 as a Senior Lecturer and currently leads the Nanotechnology and Bio-Engineering Research Group. His research interests include the synthesis of nanomaterials for energy and environmental applications. He is the recipient of a number of awards including the Boyle-Higgins Award 2019. He is an associate editor for the Chemical Engineering Journal and editorial board member for Applied Catalysis B.